

Marsh Recession and Erosion study of the Fraser Delta, B.C., Canada from Historic Satellite Imagery

Marijnissen, Richard; Aarninkhof, Stefan

Publication date

2017

Document Version

Final published version

Citation (APA)
Marijnissen, R., & Aarninkhof, S. (2017). *Marsh Recession and Erosion study of the Fraser Delta, B.C., Canada from Historic Satellite Imagery.* (Communications on Hydraulic and Geotechnical Engineering; Vol. 2017-1, No. 1). Delft University of Technology.

Important note

To cite this publication, please use the final published version (if applicable). Please check the document version above.

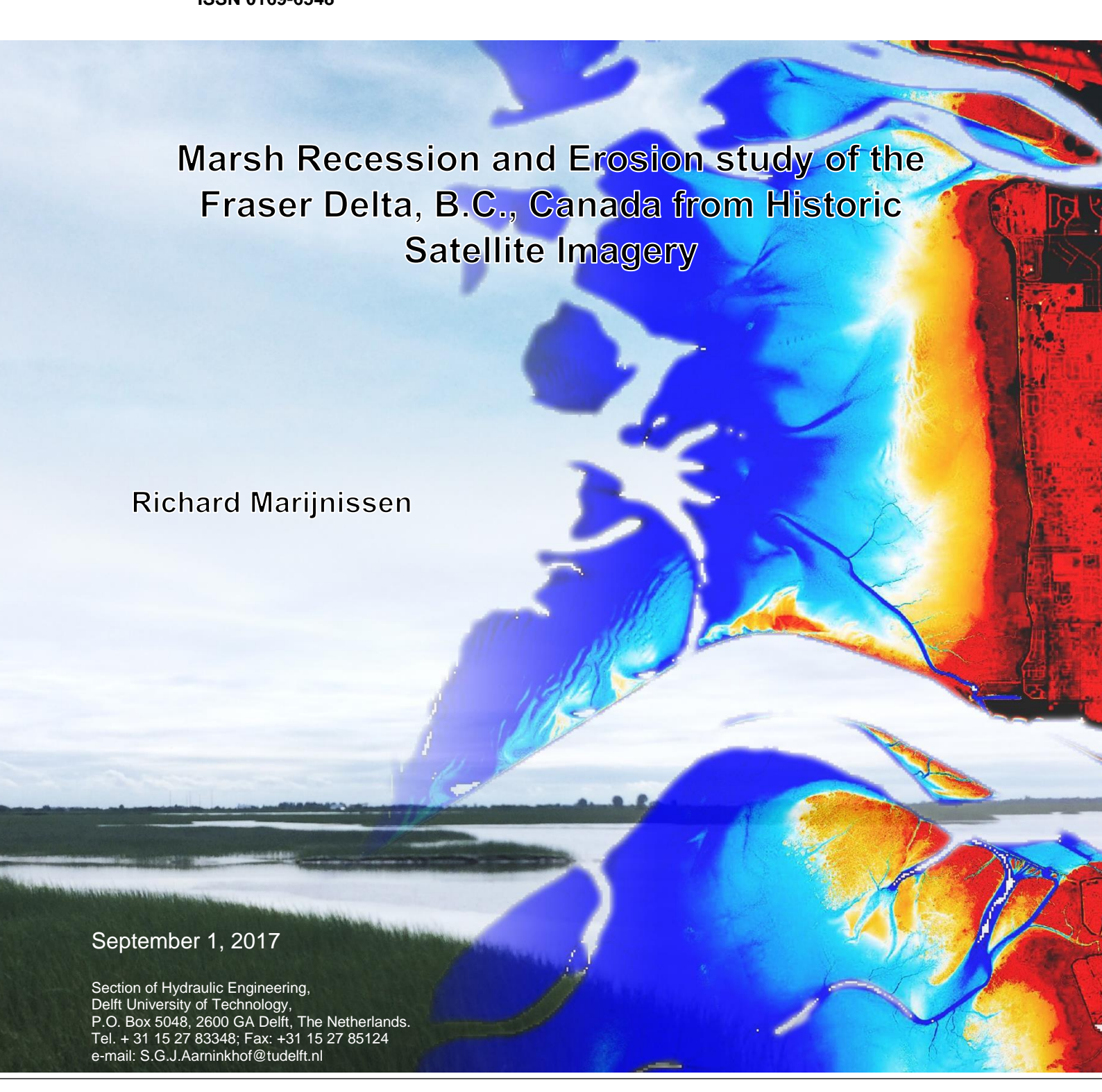
Other than for strictly personal use, it is not permitted to download, forward or distribute the text or part of it, without the consent of the author(s) and/or copyright holder(s), unless the work is under an open content license such as Creative Commons.

Please contact us and provide details if you believe this document breaches copyrights. We will remove access to the work immediately and investigate your claim.



Communications on Hydraulic and Geotechnical Engineering 2017-01

ISSN 0169-6548





Communications on Hydraulic and Geotechnical Engineering 2017-01

ISSN 0169-6548

The communications on Hydraulic an Geotechnical Engineering are published by the Department of Hydraulic Engineering at the Faculty of Civil Engineering of Delft University of Technology. In the first years mainly research reports were published, in the later years the main focus was republishing Ph.D.-theses from this Department. The function of the paper version of the Communications was to disseminate information mainly to other libraries and research institutes. (Note that not all Ph.D.-theses of the department were published in this series. For a full overview is referred to www.hydraulicengineering.tudelft.nl ==> research ==> dissertations).

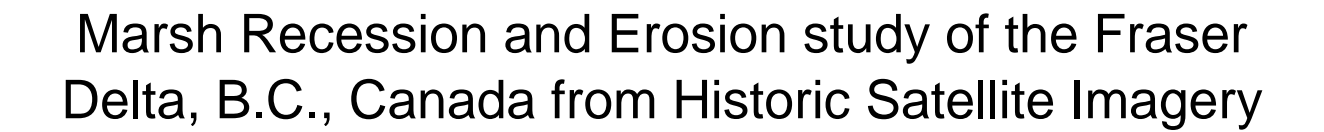
At this moment this series is mainly used to disseminate background information related to other publications (e.g. data reports with data underlying journal papers and Ph.D. theses). Recent issues of the Communications are only available in digital format. A notification will be sent to interested readers when new issues are released. For placement on the notification list, please send an e-mail to h.j.verhagen@tudelft.nl.

Older versions (before 1986) were published as <u>Communications on Hydraulic Engineering</u>.

A number of <u>internal reports</u> were not published in this series, but are also available via this website.

Postal address for the Communications is: TU Delft, Faculty of Civil Engineering and Geosciences, department of Hydraulic Engineering, Stevinweg 1, 2628CN Delft, Netherlands. Permissions for republishing parts (figures, data), can be obtained from the responsible publisher, <u>ir.</u> H.J. Verhagen

© 2017 TU Delft, Department Hydraulic Engineering; Richard Marijnissen



Written by: Ir. R.J.C. Marijnissen

Prof.dr.ir. S.G.J. Aarninkhof

September 1, 2017

Acknowledgements

This research was supported by the Vancouver Fraser Port Authority, Environment Canada and the Ministry of Forests, Lands, Natural Resource Operations and Rural Development of British Columbia.

I want to thank Eric Balke (British Columbia Conservation Foundation) and Sean Boyd (Environment Canada) who have contributed a great deal to this project with their personal experience and knowledge of the brackish marshes in the Fraser Delta. Their observations were a key part of this study.

A large part of this study was only possible with the collaboration with Deltares and the university of Cádiz. Thanks to Mindert de Vries (Deltares) I was able to learn about their ongoing efforts to use satellite imagery for assessing flood safety of natural foreshores in by connecting me to their MI-SAFE project. During the two weeks in Spain Edward Morris (University of Cádiz) was of great help by teaching me how to analyze large amounts of satellite images and going out of his way to help and work out the procedures within the study.

Richard Marijnissen, 2017

Table of contents

Α	cknowl	edge	ements	i
T	able of	cont	ents	ii
1	Intro	oduc	tion	1
	1.1	Prol	blem description	1
	1.2	Obj	ective	2
	1.3	App	roach	2
2	Met	hods	3	3
	2.1	Sate	ellite imagery	3
	2.2	Ima	ge selection	3
	2.3	Join	tidal elevation	5
	2.4	Indi	ces	8
	2.5	Met	hods for tidal flat elevations	11
	2.5.	1	Water line method	11
	2.5.	2	FAST	13
	2.6	Met	hods for marsh detection	14
	2.6.1		Spectral unmixing	14
	2.6.	2	Supervised classification	17
3	Vali	datio	on	19
	3.1	Tida	al flat elevation	19
	3.1.	1	Methodology of validating elevations	19
	3.1.	2	Results	21
	3.1.	3	Discussion	26
	3.1.	4	Best method	27
	3.2	Vali	dation of the marsh extent	28
	3.2.	1	2015 GPS marsh edge	28
	3.2.	2	1981 marsh survey	29
	3.2.	3	2017 field observation	31
	3.2.	4	Discussion	33
4	Res	ults	and discussion	34
	4.1	Tida	al flat elevation	34
	4.2	Mar	sh extent	36
	4.3	Mar	sh and elevation changes	38
	4.4	Disc	cussion of the results	40
	4.4.	1	Tidal flat elevation	40
	4.4.	2	Marsh extent	41

	4.4.3	Correlation between erosion and recession	41
5	Summa	ry and Conclusions	42
6	Referen	ces	43
App	endix: A	Image dates and water levels	A-1
App	endix: B	Pixel survey June, July 2017	B-1
Р	lot A		B-1
Р	lot B		B-2
Р	lot C		B-3
Р	lot D		B-5
Р	lot E		B-5

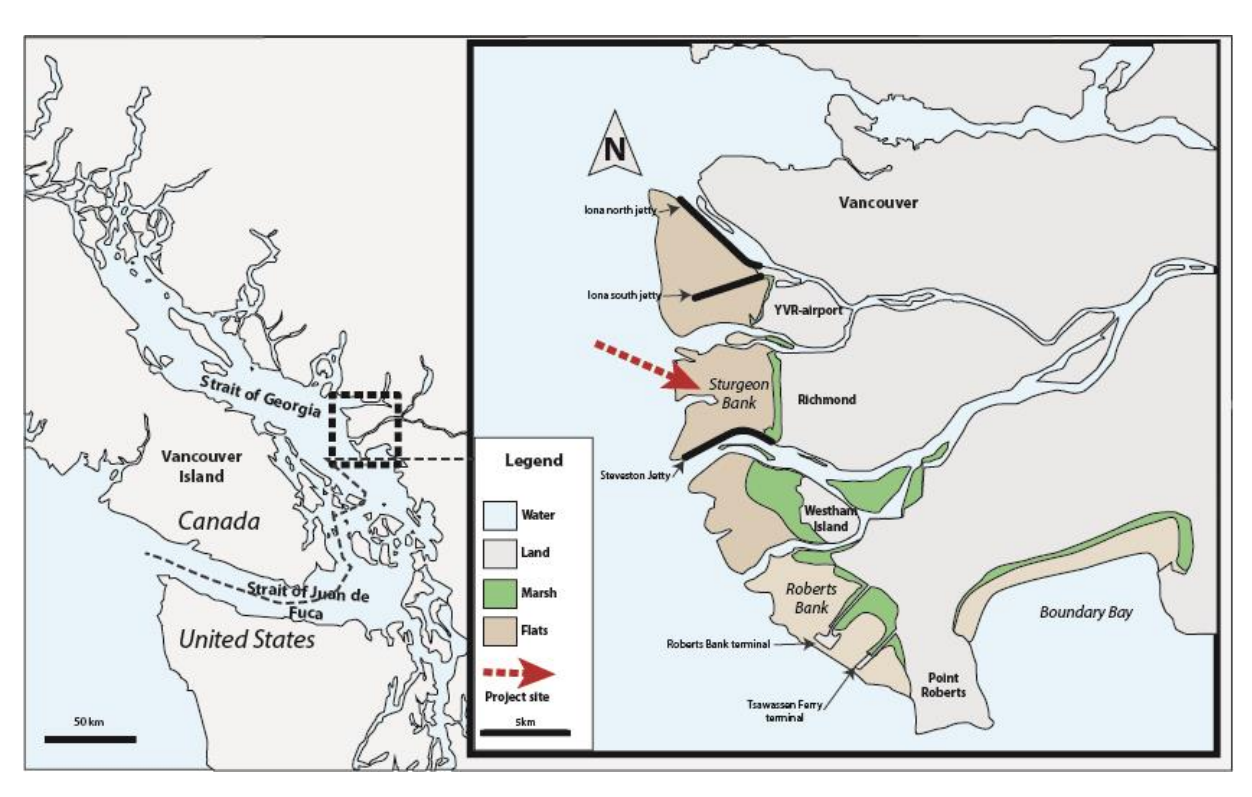


Figure 1: Location of Sturgeon Bank. Figure copied from: Potential mechanisms for the salt marsh recession on Sturgeon Bank (p. 2), Marijnissen, R., 2017, Delft.

1.1 Problem description

At the western edge of the Fraser Delta lie Sturgeon and Roberts Bank. This vast inter-tidal area is an important ecosystem of the delta. The daily exchange of tidal water from the Strait of Georgia on the shallow fore slope of the delta have allowed productive marshes to develop. These provide food and shelter for fish and millions of migratory birds flying between breeding grounds in the north and wintering grounds in the south annually. Because of these functions the area is of high ecological significance on an international level. It is designated as a Wildlife Management Area and protected by the B.C. the Ministry of Forests, Lands, Natural Resource Operations and Rural Development (Ministry of Forests, 2015).

Human activity is widespread within the Delta and it has had a profound impact on the area. Since 1905 dikes have been constructed along the river and sea (Richmond, 2005). Jetties were constructed in the 1930's and the Fraser River is being dredged to accommodate shipping. According to Hales (2000) following the construction of the jetties (1930-1954) there had been rapid expansion of marsh on Sturgeon Bank at lee side of the Steveston South jetty, while the patches of marsh on Westham Island expanded to form a more continuous marsh. Possibly the calmer conditions provided by the jetties promoted sedimentation which led to this expansion. Hales found, based on interpretation of aerial photos, that the marshes have been stable or growing until 2004, with one exception at the north side of Sturgeon Bank (Church & Hales, 2004; Hales, 2000).

There is however strong evidence that the marsh has receded. Despite initial accretion, sedimentation rates across all marshes have decreased by half between 1954 and 1994, from roughly 1 cm/year to 0.5 cm/year (Hales, 2000; Williams & Hamilton, 1995). It is

believed that dredging and redirection of the outflow from the Fraser River have limited the sediment supply to the marsh (Atkins, Tidd, & Ruffo, 2016). The most compelling evidence for marsh recession was found from the field measurement of stem density within the marsh made by S. Boyd in 1989 and in 2011. A designated plot from 1989 at the south of Sturgeon Bank fronting Steveston Road was devoid of marsh when the measurement was repeated in 2011, indicating a severe recession must have occurred within this period (S. Boyd, McKibbin, & Moore, *Unpublished*). Meanwhile the plots on Westham did not show recession, but overall stem densities had decreased significantly (by 32% averaged across all 5 plots on Westham Island).

Since the recession was discovered more efforts have been made to monitor the marshes and more evidence has come forward of recession. Historic documented marsh extents (Hutchinson, 1982; Medley & Luternauer, 1976) do not match the recently measured marsh extent (Mason, 2016, *pers. communication*). More evidence was discovered when dead corms of marsh plants were found on the bare tidal flat (Balke, 2017). Finally an examination of LandSat satellite imagery revealed a similar recession trend for Sturgeon Bank (Marijnissen, 2017).

The factor(s) causing the major loss of brackish marsh have not yet been determined but potential drivers have been suggested such as: elevated salinity levels during a historically low river outflow, sea level rise, higher sea levels due to decadal oscillations in the Pacific and a sediment deficit. It is yet unclear when the recession started, at what rate the marsh receded and if it continues to recede.

1.2 Objective

The goal of the study is to map the changes of marsh extent and topography on both Sturgeon Bank and Westham Island between 1980 and now. The study will look for a correlation between the recession and the possible loss of sediment from the banks. If a sediment deficit is a (major) contributor of marsh recession within the Fraser Delta, the results of the study should reveal such a connection.

1.3 Approach

Although there are plenty of studies suggesting changes have taken place in the marshes fronting the Fraser Delta (Atkins et al., 2016; Balke, 2017; S. Boyd et al., *Unpublished;* Hales, 2000; Williams & Hamilton, 1995), no study has utilized the extensive data record of satellites to study these changes for the entire Fraser Delta. Tools like the Aquamonitor (Donchyts et al., 2016) can detect the changes in coastlines in the past 30 years from satellite imagery. More advanced tools are still in development like MI-SAFE, which detects inter-tidal elevations and vegetation on foreshores to estimate the potential risk reduction of flooding by coastal vegetation all across the world (FAST, 2017). Within the study the latest techniques from these tools are applied and adapted to the Fraser Delta. By using the full 30+ years of information on satellite imagery, the marsh and inter-tidal surface changes are examined from a new angle.

2.1 Satellite imagery

The main source of data for the study has been satellite imagery from LandSat and Sentinel. These are space programs from NASA and the U.S. Geological Survey, and the European Space Agency (ESA) respectively that monitor the earth's surface through spectral images. The satellites orbit the earth at an altitude of 705 km covering 185 km wide swaths during each pass. Every 16 days the satellites cross the same point above the earth and thus produce an image for any location at a 16-day interval (U.S. Geological Survey, 2015). The LandSat program has a long history of successive missions. Only LandSat 5, 7 and 8 are used since they cover the period of interest (1980-2016) in the greatest detail. Higher resolution Sentinel imagery is available since 2015.

The images were retrieved and processed using the Google Earth Engine, a large-scale cloud computing platform for planetary remote sensing (Gorelick et al., 2017). Each image had already been orthorectified and processed to top of atmosphere reflectance (TOA) by the data provider. The use of these orthorectified TOA images reduces the variability between different scenes by compensating for solar angle, exoatmospheric solar irradiance and variability in the distance between the earth and sun (Chander, Markham, & Helder, 2009).

Table 1 Sources of the satellite image	Table 1	Sources	of the	satellite	image
--	---------	---------	--------	-----------	-------

Source	Provider	Name	Image collection ID	Date range	Resolution [m]
Google Earth Engine	USGS	USGS Landsat 5 TM TOA Reflectance (Orthorectified)	'LANDSAT/LT5_L1T_TOA'	Jan 1, 1984 - May 5, 2012	30
Google Earth Engine	USGS	USGS Landsat 7 TOA Reflectance (Orthorectified)	'LANDSAT/LE7_L1T_TOA'	Jan 1, 1999 – May 5, 2003*	30
Google Earth Engine	USGS	USGS Landsat 8 TOA Reflectance (Orthorectified)	'LANDSAT/LC8_L1T_TOA'	Apr 11, 2013 – ongoing	30
Google Earth Engine	EU/ESA/Copernicus	Sentinel-2: MultiSpectral Instrument (MSI), Level- 1C	COPERNICUS/S2	Jun 23, 2015 – ongoing	20

^{*}LandSat 7 is still operational, but due to a malfunction suffers from striping, i.e.images contain swaths of missing information. Images after May 2003 are therefore not considered

2.2 Image selection

The total amount of raw satellite images covering the area of interest in the collection is 977 images. Upon closer inspection however, many of these images are unsuitable for analysis due to a large amount of cloud cover. Dense clouds not only obscure the view of the flats and marsh underneath them, but also cast shadows that change the appearance of the features. Because a computer will look for spectral similarities on the image, the area affected by the shade will not be recognised as the same class as the area outside of the shade. Veils of translucent clouds pose the same problem as shadows. The translucent



Figure 2 The Fraser Delta as seen on a cloudy LandSat true-color composite, left without clouds and right with an estimated cloud cover of 26.64%. Data made available by the USGS.

clouds whiten the area such that a computer cannot recognise its class. Examples of these situations are present in figure 2.

Cloud cover on each image is estimated by the data provider with a dedicated algorithm. Cloud pixels are classified under the premise that clouds tend to be bright and cold compared to the surroundings (Irish, 1999). The estimated cloud cover follows as the percentage of pixels identified as cloud from the total number of pixels in the image. Algorithms are available for filtering pixels affected by clouds out of the image. However water pixels that are both cold and bright (e.g. in turbid water) can be misclassified as clouds (Zhu, Wang, & Woodcock, 2015).

Because of the complications that arise from using cloudy images a conservative approach is taken. All images with an estimated cloud cover of over 10% are filtered out of the collection. The LandSat and Sentinel collection is reduced from 977 to 156 images for the area of interest in the period 1980 to the first of July 2017.

Even with the strict cut-off of 10% cloud cover, clouds can still be present within the image. Using the premises stated before that clouds tend to be bright and cold, algorithms have been developed by the earth engine community to filter out cloud pixels from an image with a simple cloud score (Herwig, 2016; Housman, 2016). These algorithms were implemented to ensure occasional clouds would not significantly affect the results of the study. As shown in figure 3 and figure 4 the cloud filtering is quite conservative on cloudy images, but did not affect cloud free images. The cloud removal acts more like an additional filter that inhibits potentially problematic classification on cloudy images, rather than to accurately remove clouds.



Figure 3 True-color composite of an image with less than 10% cloud cover before simple cloud filtering

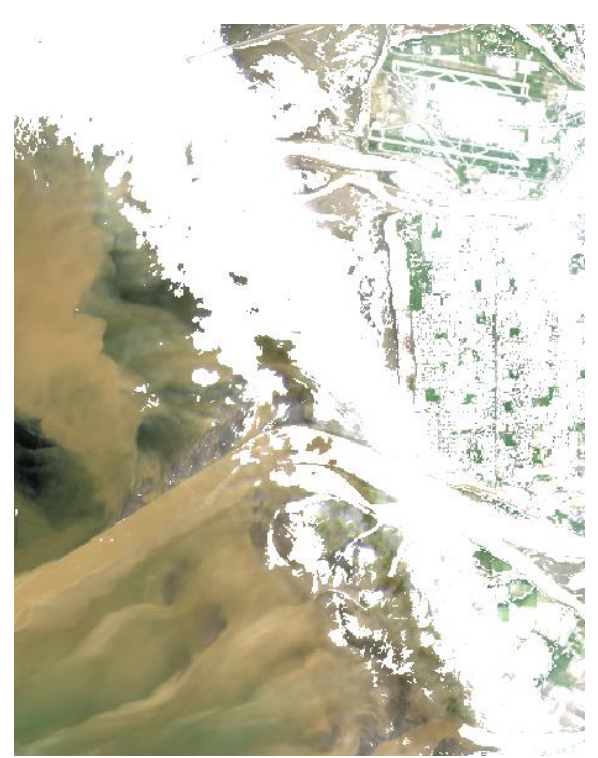


Figure 4 True-color composite of an image with less than 10% cloud cover after simple cloud filtering

2.3 Join tidal elevation

In order to detect the vegetation and marsh on the images in the collection, the tidal elevation on each image needs to be known. Elevation on the satellite images can be estimated from the water lines on the images while marsh can only be seen when it is not submerged by the tide. The elevation of the tide is thus a crucial piece of metadata for the process.

Hourly water levels for the entire period of interest (1985 to now) were retrieved from the Point Atkinson Tide Gauge Station. It is located about 20 km north of Sturgeon Bank and 25 km north of Westham Island (Figure 6). At this location, there is a continuous record of hourly water levels for the entire period. Hourly water level records closer to Sturgeon Bank and Westham Island are only available from Sand Heads Tide Gauge Station for a limited period (09 Feb 2006 to 27 Sep 2006). The water levels recorded at Point Atkinson can be converted to water levels at the Sand Heads by fitting the 2 datasets. Because the tide within the Strait of Georgia exhibits a standing wave pattern (Thomson, 1981), there is a strong similarity in timing between the two locations.

The water level at Sand Heads indeed has a strong correlation with the water level at Point Atkinson (Figure 5). A linear function was fitted to the two datasets by applying model 2 regression.

Eq. 1
$$h_{SandHeads} = 0.9746 * h_{P,Atkinson} + 0.1695$$

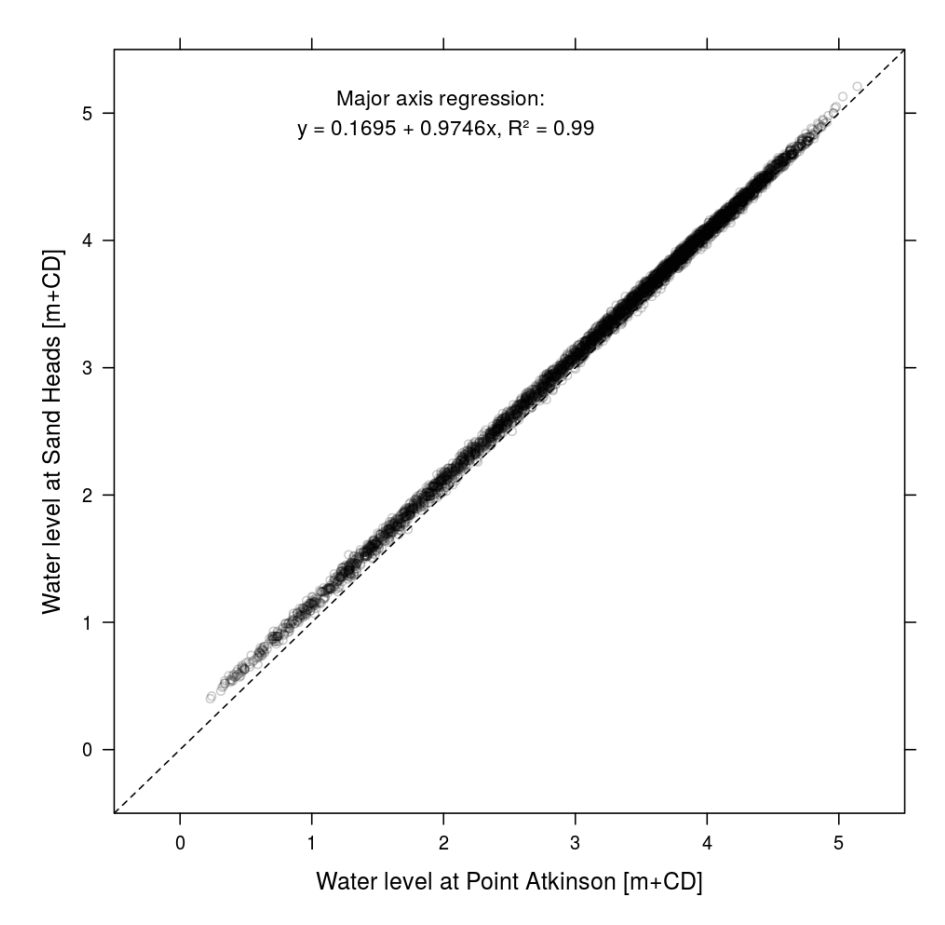


Figure 5 Relation between the water level at Point Atkinson and Sand Heads

With eq.1 the water levels between 1985 and 2016 at the Sand Heads were calculated. Since the coefficient of determination (R²) of the function is very close to 1, there is great confidence the calculated water levels reflect the actual historic water levels at that location.

From the satellite metadata the exact date and time each image was taken is known. The date of each image within the collection was exported from the Google Earth Engine into a table. To calculate the water level at each time in the table the water levels at the two nearest full hours were retrieved from the Point Atkinson tide gauge and converted to water levels at the Sand Heads with eq. 1. The water level at the time of the image is then interpolated from these two water levels (eq. 2).

Eq. 2
$$h_{t_{image}} = h_{t1} + \frac{h_{t2} - h_{t1}}{60} * t$$

$$h_{t_{image}} = Water level at time t (moment of image, e.g. at 18:25)$$

$$h_{t1} = Water level at the nearest hour rounding down (e.g. at 18:00)$$

$$h_{t2} = Water level at the nearest hour rounding up (e.g. at 19:00)$$

$$t = Time in minutes between t_{image} and t_1 (e.g. 25)$$

The dataset of Point Atkinson is extensive but there are moments of missing data. This affected only 2 out of the 156 images. A predictive tide model (Stephenson, 2016) was fitted to the dataset and calculated the water level if no data was found from the tide gauge.

Table 2 Details for Point Atkinson Tide Station

Point Atkinson, B.C. #7795

Provider: Fisheries and Oceans Canada

Latitude 49.337° N

Decimal Degrees:

Longitude 123.253° W

Decimal Degrees:

Datum: CD
Time Zone: PST

Status: PERMANENT

Alternate Caulfeild Cove, Sandy Cove

Station Name:

Established: 1897
Province: BC
Ownership: PAC
Tide Table 5

Volume:

Geo Location: STRAIT OF GEORGIA

URL <a href="http://isdm-gdsi.gc.ca/isdm-gdsi.

gdsi/twl-mne/inventory-inventaire/sd-ds-

eng.asp?no=7795&user=isdm-

gdsi®ion=PAC

Table 3 Details for Sand Heads tide gauge

Sand Heads, B.C. #7594

Provider: Fisheries and Oceans Canada

Latitude 49.125° N

Decimal

Degrees:

Longitude 123.195° W

Decimal Degrees:

Datum: DPWD

Time Zone: PST

Status: TEMPORARY

Established: Province: BC
Ownership: PAC
Tide Table 5

Volume:

Geo Location: FRASER DELTA

URL <a href="http://isdm-gdsi.gc.ca/isdm-gdsi.

gdsi/twl-mne/inventory-

inventaire/sd-ds-

eng.asp?no=7594&user=isdmgdsi®ion=PAC&ref=maps-

cartes



Figure 6 Locations of the Point Atkinson and Sand Heads tide gauges as reported by Fisheries and Oceans Canada on Google maps

The updated table (see Appendix: A) with the dates of the images and the tidal elevation was imported into the Google Earth Engine. A function was written within the Earth Engine to add the tidal elevation as metadata to the image with the same timestamp. The collection with water levels is then available for further processing.

The percent of time an intertidal elevation is visible on an image given the tidal heights at Sand Heads is visualised in figure 7. Elevations below 0.5 m+CD will almost always be under water while land above 5 m+CD will always be above water. Areas with an elevation of 3.2 m+CD are expected to be exposed on half of the images in the collection.

Table 4 Tidal heights at Point Atkinson and Sand Heads with reconstructed heights for Sand Heads for the period 1985-2016. Original data from Canadian Hydrographic Service, data processed with tidal harmonics package (Stephenson, 2016)

	Point	Sand Heads
	Atkinson	1985-2016
	1985-2016	[m+CD]
	[m+CD]	
HHW	5.52	5.55
MHHW	5.37	5.40
MLHW	3.53	3.60
MWL	3.11	3.20
MHLW	2.69	2.79
MLLW	0.85	1.00
LLW	-0.24	-0.06

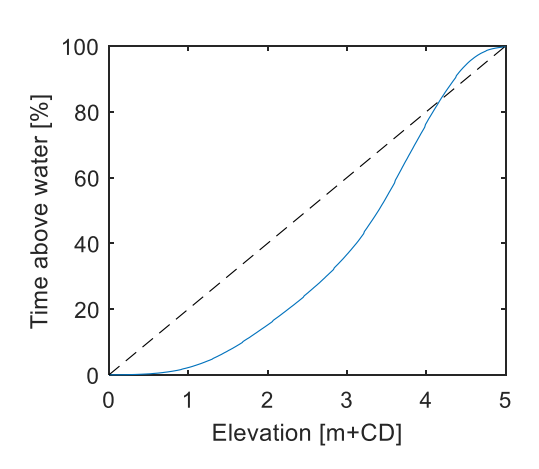


Figure 7 The fraction of time each elevation is exposed by the tide at the Sand Heads

2.4 Indices

The satellite images are recorded with different spectral bands. Each band represents sensors that measure the radiation within specific wave lengths. The red, blue and green channels make up the visual spectrum, but more bands are available across all satellites to detect land and marsh features. Bands should be used in which the features that need to be identified are most distinct.

Live biomass on the tidal flats can be detected by the absorption of red and reflectance of infrared wavelengths due to chlorophyll inside the plants (Hardisky, Daiber, Roman, & Klemas, 1984). Water can be detected across different bands though near-infrared (NIR) and short-wave infrared (SWIR) are most effective (Ryu, Won, & Min, 2002).

To study vegetation and water features consistently across different conditions, dedicated indices have been developed that rescale the radiance of one or multiple bands into a normalized index in which these features show contrasting values with their surroundings. Indices used within the study are presented in

table 6.

The result of the conversion to a normalized index is a grey-scale image with values scaled between -1 and 1, on which features are more easily identifiable than any individual band (Figure 8). In the Google Earth Engine the different indices were calculated for each image in the available LandSat and Sentinel collection covering the area of interest between 1980 and 2017.

Table 5 Spectral bands per satellite

	Landsat 4-5 (TM)	Landsat 7 (ETM+)	Landsat 8 (OLI)	Sentinel 2
Band 1	Blue	Blue	Ultra Blue (coastal/aerosol)	Coastal aerosol
Band 2	Green	Green	Blue	Blue
Band 3	Red	Red	Green	Green
Band 4	Near Infrared (NIR)	Near Infrared (NIR)	Red	Red
Band 5	Shortwave Infrared (SWIR) 1	Shortwave Infrared (SWIR) 1	Near Infrared (NIR)	Vegetation Red Edge
Band 6	Thermal	Thermal	Shortwave Infrared (SWIR) 1	Vegetation Red Edge
Band 7	Shortwave Infrared (SWIR) 2	Shortwave Infrared (SWIR) 2	Shortwave Infrared (SWIR) 2	Vegetation Red Edge
Band 8		Panchromatic	Panchromatic	NIR
Band 9			Cirrus	Water vapour
Band 10			Thermal Infrared (TIRS) 1	Cirrus
Band 11			Thermal Infrared (TIRS) 2	SWIR 1
Band 12	<u> </u>	<u> </u>		SWIR 2

Table 6 Indices computed from LandSat and Sentinal spectral bands

Abbreviation	Bands used*	Formula	Full name	Reference
NDVI	R, NIR	$\frac{NIR - R}{NIR + R}$	Normalized difference vegetation index	-
NDWI	G, NIR	$\frac{NIR - G}{NIR - G}$	Normalized difference water index	(McFeeters, 1996)
MNDWI	G, SWIR1	$\frac{SWIR1 - G}{SWIR1 + G}$	Modified normalized difference water index	(Xu, 2006)
CNDSI	G, R, NIR, SWIR1	$\frac{NDVI + NDWI + MNDWI}{3}$	Combined normalized difference surface index	-

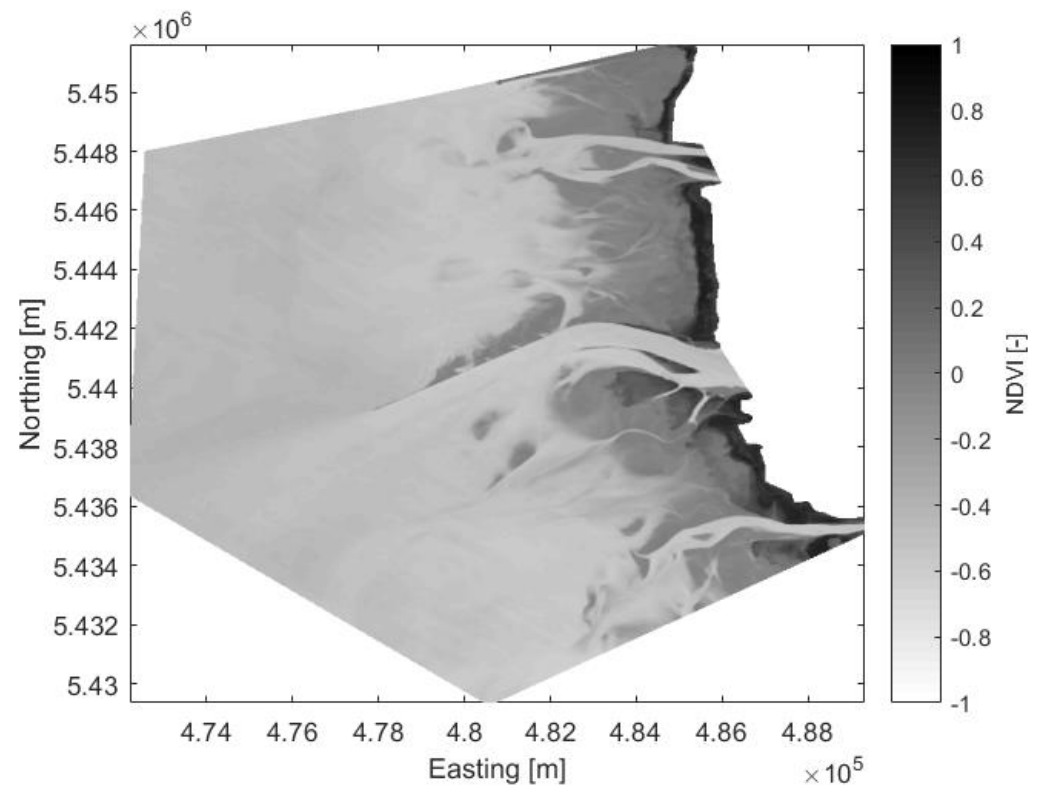


Figure 8 Example of a NDVI image. Light colors indicate water while dark colors are indicative of plant cover.

One more step is taken to find edges between features. Water, in most cases, will appear the same across the same image, hence the value of the calculated index will vary only slightly. However, the appearance of water and land is very different and thus the value of the calculated index will change significantly at the water-land boundary. The sudden transition from bare or sparsely vegetated flat to an area with dense plant cover will have the same effect. The edges between features can thus be delineated by steep gradients within the index.

In Google Earth Engine, the x- and y-gradients are computed in pixel coordinates, each using a simple 3x1 kernel. Then the same 3x1 kernels are used to compute the gradients of easting and northing as the final physical gradient in units, unaffected by the projection of the image. Finally, the magnitude of the gradient is calculated with the Pythagorean theorem from the x- and y-gradients.

Depending on the sensitivity of the index to certain features the gradients become more or less pronounced. For example, the suspended sediment in the water near the tidal flats can blur the otherwise clear transition for one feature (e.g., water) to the other (e.g., land). In interpretation this is helpful as greater certainty can be attributed to greater gradients. On the other hand, if an image contains a large amount of noise or disturbances (e.g., sun glint or clouds), edges are found that do not reflect any physical edges between features on the tidal flat.

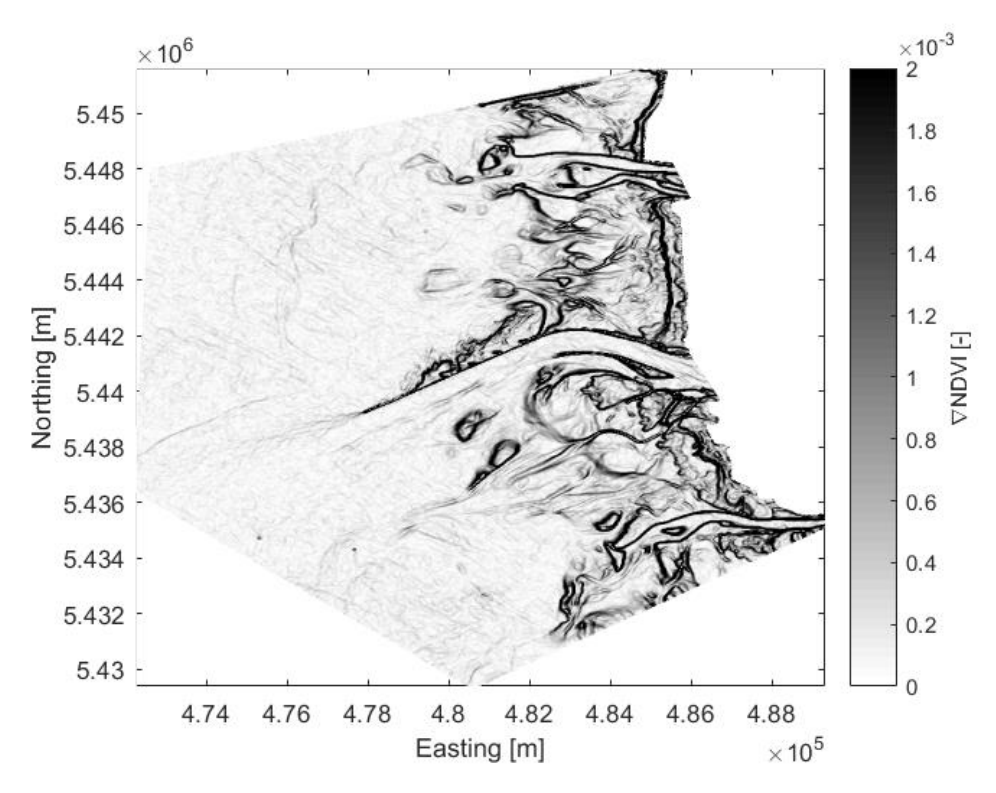


Figure 9 The gradient image calculated from figure 8. Large gradients (black) are indicative of edges between features such as water, land and dense marsh.

2.5 Methods for tidal flat elevations

2.5.1 Water line method

Elevation models of the coast can be constructed through remote sensing by detecting the water line at various times during the tide (D. C. Mason, Davenport, Robinson, Flather, & McCartney, 1995; Murray, Clemens, Phinn, Possingham, & Fuller, 2014; Ryu et al., 2002). The key assumption of this method is that the water lines on the images are at the same elevation as the tidal height (measured or modelled) at that time. Essentially the water lines become contour lines at the elevations of the observed stages of the tide.

The most important part of the analysis is defining when a pixel on an image should be classified as a water line. The easiest definition would be using a threshold. Any value of the normalized difference surface index (NDSI) below the threshold is classified as water while any value above the threshold is considered land. Indices, however, can still vary from image to image for the same class due to atmospheric conditions. A single threshold will therefore not be suitable for all images.

To resolve this the gradient of the NDSI is taken into consideration. Transitions from water to land should show a rapid change in the index as the spectral characteristics of the surface change. A range within the NDSI is defined in which the transition can be expected. Within the range only the pixels that exceed the gradient threshold are considered a water line. The water line is thus defined by:

NDSI > water threshold
 NDSI < land threshold
 Gradient of NDSI > threshold
 Values below this threshold is very likely to be land.
 Values above the threshold is very likely to be land.
 Values below this threshold are too small for an edge

The values of the thresholds were estimated by hand from a number of images for each NDSI in table 6. The water and land thresholds were determined by estimating the position of the water line visually and sampling points about 10 pixels around this estimated edge. The highest and lowest sampled values were then rounded to rough estimates and implemented as a threshold. The gradient threshold was estimated by gradually increasing the value until most noise was filtered out, but lowered when water lines were being lost. The final values are presented below in table 7.

NDVI was affected by noise most but did not have as steep gradients as other indices. This inhibited the filtering of all noise by increasing the gradient threshold as water lines would be lost. NDWI showed a larger difference between water and land which allowed for both a higher land and gradient threshold. MNDWI was very sensitive to water, but it only detected water edges more landward than the other indices. CNDSI showed the highest land to water gradient and thus the gradient threshold could be set higher. Even though the gradient was high, the actual value at the landward side remained lower compared to other indices which necessitated a land threshold similar to the NDVI.

Table 7 Thresholds used to define a water line per index

	Water threshold	Land threshold	Gradient threshold
NDVI	-0.25	-0.15	0.75E-3
NDWI	-0.25	0	1.5E-3
MNDWI	-0.5	-0.2	1.5E-3
CNDSI	-0.25	-0.15	1.75E-3

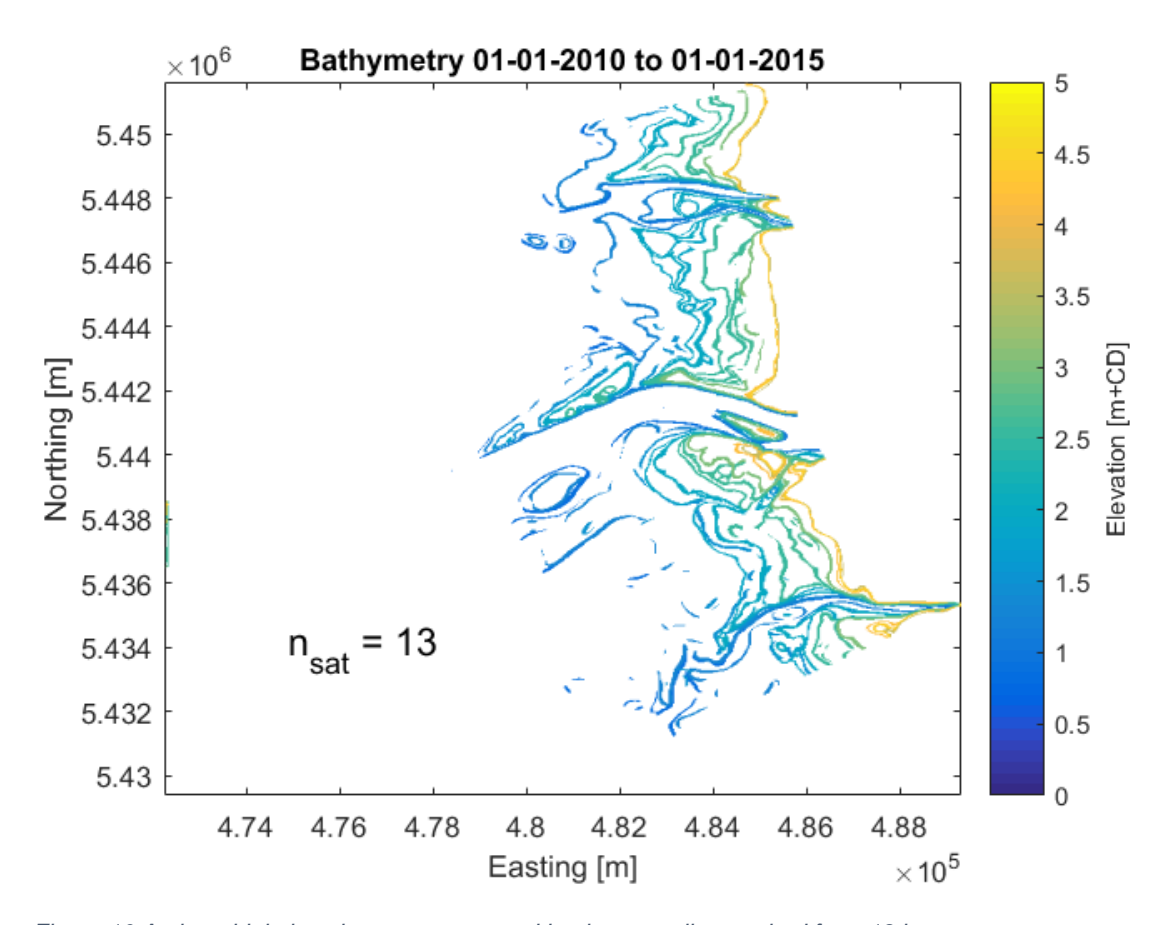


Figure 10 An intertidal elevation map generated by the water line method from 13 images

Each water line pixel in an image is assigned the value of the tidal elevation. The resulting collection consists of 156 images, each with a water line that serves as a contour line of one elevation at one date and time. This collection should then be filtered for dates within the period of interest. All water lines from the period are combined into one image. Where water lines overlap the elevation is averaged. The result is an image of contour lines at different elevations (Figure 10). If more images are available a more detailed bathymetry can be constructed.

2.5.2 FAST

The FAST (Foreshore Assessment using Space Technology) methodology is still in development and will be improved in the future. Because of this not all details of the method can be given until the methodology is published. However, the principles of the methodology are explained below.

In FAST the elevation is estimated by calculating the probability of inundation of each pixel (FAST, 2017). The process first generates a time-averaged image of the selected water-index (MNDWI for this study, but could be changed in the future). The process will be explained further using the NDVI image of figure 8 as an example.

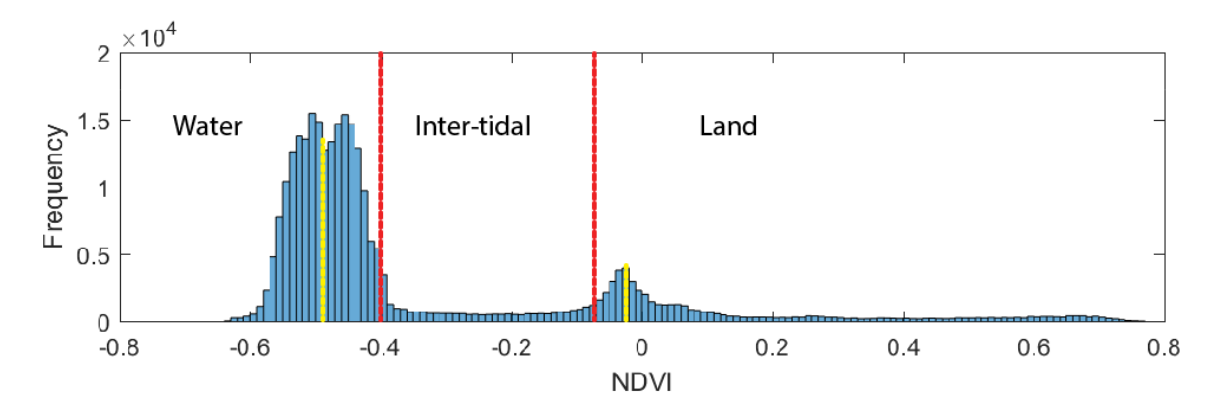


Figure 11 Visualisation of the classification of the inter-tidal zone in FAST

From the time averaged image a classification algorithm is used to split the image into 2 classes, water and land, and finds the corresponding index values. This classification is done by looking for the peaks of land and water within the histogram of the image. The index values in between the distributions for land and water can be interpreted to have been water on some images, and land on others. The probability of inundation is calculated from a probability distribution between the optimal water and land class index values.

The resulting probability of inundation is then scaled linearly to the highest and lowest astronomical tide. An inundation probability of 100% means the area is lower than the lowest astronomical tide as it is always under water while an inundation probability of 0% is higher than the highest astronomical tide (FAST, 2017). The elevation is equal to the tidal elevation of submergence and so an inter-tidal bathymetry is constructed.

2.6 Methods for marsh detection

Before the marsh can be detected it must be ensured that it is visible on the images. First the collection is filtered for low tide images (tide levels below 1.2 m+CD). On the low tide images the marsh is not obscured by the tide and is detected more easily. Additionally, only images from the summer when the marsh is at peak growth, should be considered. Different plants have peak growth and start scenesing at different times of the summer. Plants of the same species but in different areas can also peak/scenese at different times. However, limiting the date range further would severely limit the amount of images that can be used. The remaining images in the collection thus satisfy the criteria:

- Less than 10% cloud cover
- Taken at a tide lower than 1.2 m
- Taken between 1st of July and 31st of August

The criteria severely limit the collection to only 17 images covering the period 1980 to 2017.

The detection of marsh requires more complicated methods than were needed to detect water (edges). The spectral differences between water and land are quite big compared to the difference between tidal flat and the transition into (sparse) marsh. As a result the specific characteristics to differentiate between the two from a spectral band or index are not obvious. The methods introduced in this section are chosen because of their ability to be trained to detect smaller spectral differences and use it to find the marsh.

2.6.1 Spectral unmixing

One of the simpler methods that trains to find the criteria of predefined classes as marsh is spectral unmixing. Spectral unmixing is a technique in remote sensing whereby the total spectral signal of a pixel is decomposed into components (Van Der Meer, 1995). Rather than a single 30x30m LandSat pixel being just water, flat or marsh, the signal from the pixel is most likely a combination of the three. With spectral unmixing the fraction of each class contributing to the signal is calculated.

The number of classes must be equal to the number of bands for this approach and the classes should be fuzzy to allow for fractional covers. Furthermore the bands should be different enough between classes to do a reliable calculation. All indices (NDVI, NDWI and MNDWI) are selected as bands to select a water, a land and a marsh class. NDVI is designed to pick up vegetation whereas NDWI and MNDWI are designed pick up water, with MNDWI being the most sensitive to changes in water content. Combined they can better differentiate between these classes.

First the NDVI, NDWI and MNDWI values for 'pure' water, flat and marsh must be defined. Training areas were chosen such that one can be certain of the class there at all times. The training area for water was chosen at the mouth of the middle arm of the Fraser River, flats were defined around 200 m offshore of the approximate marsh. On Sturgeon Bank marsh was trained in the southern portion north of Garry Slough and on Westham Island a section on the northern side was chosen. The marsh training areas include both low and high marsh (see Figure 12).



Figure 12 Training areas for spectral unmixing: blue is water, yellow is flat and green is marsh. The reference marsh fraction was found on the flat at the red marker.

The pure marsh (\bar{m}) , flat (\bar{f}) and water (\bar{w}) index values are found by averaging the values across their respective training areas:

$$\overline{\boldsymbol{m}} = \begin{bmatrix} \overline{ndvi}_m \\ \overline{ndwi}_m \\ \overline{mndwi}_m \end{bmatrix}, \quad \overline{\boldsymbol{f}} = \begin{bmatrix} \overline{ndvi}_f \\ \overline{ndwi}_f \\ \overline{mndwi}_f \end{bmatrix}, \quad \overline{\boldsymbol{w}} = \begin{bmatrix} \overline{ndvi}_w \\ \overline{ndwi}_w \\ \overline{mndwi}_w \end{bmatrix}$$

For any given pixel on the image (say at x position i and y-position j) that contains index values $(ndvi_{i,j}, ndwi_{i,j}, mndwi_{i,j})$ the marsh, flat and water fractions $(m_{i,j}, f_{i,j}, w_{i,j})$ are calculated. To do so they are rewritten into a set of linear equations:

$$\boldsymbol{c}_{i,j} = \begin{bmatrix} ndvi_{i,j} \\ ndwi_{i,j} \\ mndwi_{i,j} \end{bmatrix}, \qquad A = \begin{bmatrix} \overline{\boldsymbol{m}}, \overline{\boldsymbol{f}}, \overline{\boldsymbol{w}} \end{bmatrix} = \begin{bmatrix} \overline{ndvi}_{m} & \overline{ndvi}_{f} & \overline{ndvi}_{w} \\ \overline{ndwi}_{m} & \overline{ndwi}_{f} & \overline{ndwi}_{w} \\ \overline{mndwi}_{m} & \overline{mndwi}_{f} & \overline{mndwi}_{w} \end{bmatrix}, \qquad \boldsymbol{x}_{i,j} = \begin{bmatrix} m_{i,j} \\ f_{i,j} \\ w_{i,j} \end{bmatrix}$$

Eq. 3
$$c_{i,j} = m_{i,j} * \bar{m} + f_{i,j} * \bar{f} + w_{i,j} * \bar{w} = Ax_{i,j}$$

Eq. 4
$$x_{i,j} = A^{-1}c_{i,j}$$



Figure 13 The result of the spectral unmixing procedure for marsh classification

The set of equations is solved within Earth Engine for each pixel in the image. In a second step, the values within $x_{i,j}$ are normalized to arrive at fractions. The marsh area was found at those location with a marsh fraction greater than a threshold:

$$m_{i,i} > m_{ref} \rightarrow \text{cell is marsh}$$

The marsh fraction does not directly correspond to marsh as was implied. The marsh fraction in this approach is affected by wetness. As can be seen in figure 12, the water training area is naturally always wet, the flat training areas are lower in elevation than the marsh training area hence the flats remain wetter at low tide than the marsh. As a result, the algorithm is trained to associate dry areas with marsh.

The exposed sand ridges north of the Steveston North Jetty dry up at low tide and are thus not as wet as the flat training areas. Consequently, these flats are calculated to have a marsh fraction despite there being no marsh. The calculated marsh fraction at this location was sampled and used as the threshold value for the marsh classification.

The remaining pixel values are rescaled to values between 0 and 1. Values closer to 1 represent pixels with a greater similarity to the "pure" marsh while values closer to 0 are more different and thus less certain to be marsh.

The spectral unmixing method was applied to the time averaged images for each period including the training. Thus for each period the classifiers are recalibrated. Given the limited amount of images this was necessary to account for variations in indices from image to image that would have been averaged out in a large collection. The result of the procedure is a map where values close to 1 (green) are indicative of marsh presence (Figure 13).

2.6.2 Supervised classification



Figure 14 Training areas for the supervised classification algorithm. Blue = water, yellow = flat, red = sea grasses, dark green = high marsh, light green = low marsh

Supervised classification uses training areas of predetermined classes and looks for predictors of the class. The predictors can then be applied across other images to classify them in their entirety. Multiple automated supervised classification algorithms are available within Google Earth Engine. Of those the random forest method was found to be most promising for object-based classification according to literature (Ma et al., 2017). A random forest is a classifier consisting of a collection of tree-structured classifiers where each tree casts a unit vote for the most popular class (Breiman, 2001). The details of the method are documented by Breiman (2001).

All spectral bands (red, green, blue, NIR, SWIR1, SWIR2) and indices (NDVI, NDWI, MNDWI) could and were used within the method. Problematic areas from the unmixing approach were implemented in the training set to ensure these areas would be classified differently. Closer inspection suggested sea grass, algae and wetness were influencing the spectral unmixing results (see Discussion at Section 3.2.3), so new classes were determined. A "sea grass" class was implemented to classify green areas outside of the marsh. Further the low and high marsh were separated into two classes as the high marsh was usually more distinct on the indexed images than the low marsh.

A different approach was taken to the training areas as for the spectral unmixing approach. The classifier was trained within one period: 2010-2017. The classifier was then applied to the other images. The consideration for unmixing was that due to the limited number of images available it was better to reclassify water, flat and marsh for each period. This was manageable since the procedure is not computationally intensive and training areas could be very certain to remain that class for the entire study period. Supervised classification is more computationally intensive and the assumption of the training areas not changing classes between periods does not hold for the new classes.

The training areas are presented in figure 14. Training areas for water were selected again within the Fraser river, but with the addition of more training off-shore to account for differences between sediment content within the river and off-shore. Because the training area no longer needs to apply for the entire period, the GPS marsh edge from 2015 could be used to delineate flat and low marsh on Westham Island where classification was most difficult. A region on Sturgeon Bank with sea-grass as observed in the field in 2017 and visible on Google Earth was selected to train the algorithm to account for green cover outside of the marsh. The southern part of Sturgeon Bank was again selected to use for the classification of high marsh.

After the training was completed and the retrieved predictors were applied to the whole image, a classified map is returned (Figure 15).



Figure 15 The random forest classified image for the period 2010-2017. Dark blue areas are classified as water, light blue areas as flat, red areas as flat with possibly algae or sea grass, light green as low marsh, and dark green as high marsh

3.1 Tidal flat elevation

The results of the study are checked against other elevation measurements to establish the accuracy of the method. In this case a LIDAR survey of the area from 2013 provided by the Vancouver Fraser Port Authority was available to compare the results of this study against. The elevations were calculated from the 10-year period around 2013, 2008 until the 1st of July 2017.

3.1.1 Methodology of validating elevations

For the validation the elevations produced by the satellite methods needed to be compared against the LIDAR survey. To do so elevations were sampled in two ways: many samples taken randomly across the whole area or a small number of samples at set transects. The random samples are less likely to be affected by any outliers and give a representation of the overall accuracy of the methods. The transects on the other hand show how the errors of a method can skew elevations along the profile which is relevant for certain practical cases (e.g. calculating the flooding probability at the dike).

A large number of sample points were randomly generated across the study area. It was found 10,000 points were adequate. For each point the corresponding elevation was retrieved from the LIDAR set and the satellite set (schematized in figure 16). For the waterline method four indices were tried and thus generated four sets of elevations to verify against the LIDAR survey. The fifth set of satellite elevations was generated by the procedure from FAST.

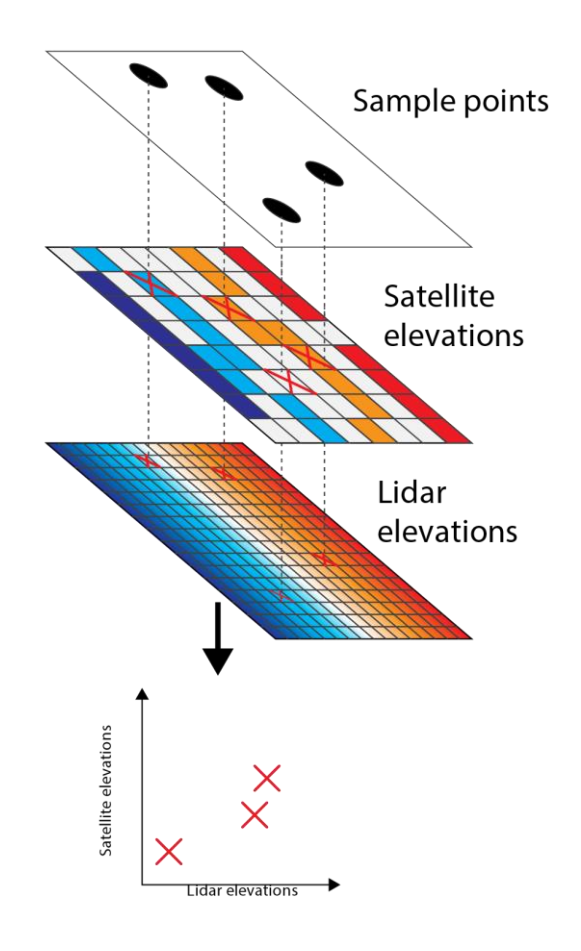


Figure 16 Procedure for validation

For many sample points no elevation could be found in one or both datasets. These points are in locations where no LIDAR is available like far off-shore or within the channel of the middle arm, or in points were water line has been detected in the study period.

As a measure of accuracy the root mean squared error (RMSE) and mean absolute error (MAE) were calculated from the N number of points that contain elevations. A graph was plotted for each method showing the relation between the predicted height from the satellite and the height measured from the lidar survey (see the results in figure 19).

After the random sampling, four transects at Sturgeon Bank and Westham Island were analysed. Many transects had been established by the Fraser River Estuary Management Program (FREMP) before. For continuity two FREMP transects at the center of Sturgeon Bank and two on Westham Island were selected: transects J, I, E, and F (see figure 17). The

original transects only had points at 200 m intervals. Additional points were added in between the original ones to reduce the intervals to 50 m and make more detailed transects.

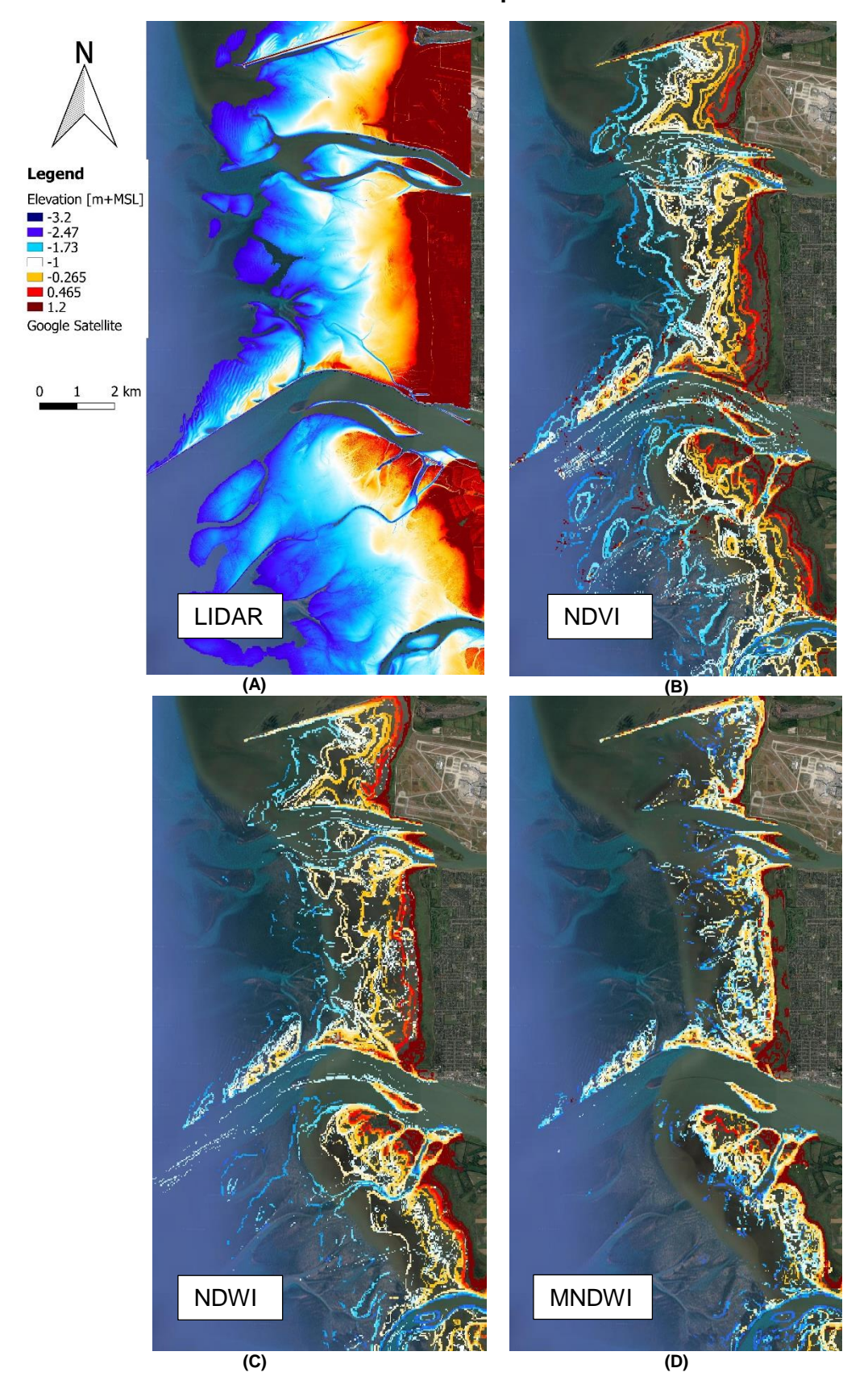
The sampling process for the transects was identical to the process described for the random samples. At each sample point on the transect the elevation was retrieved from the LIDAR survey and the elevations generated by the satellite procedures. Along each transect the RMSE and MAE was calculated for each method. The elevations are plotted along the transect to show the different elevation profiles generated by the satellite methods.

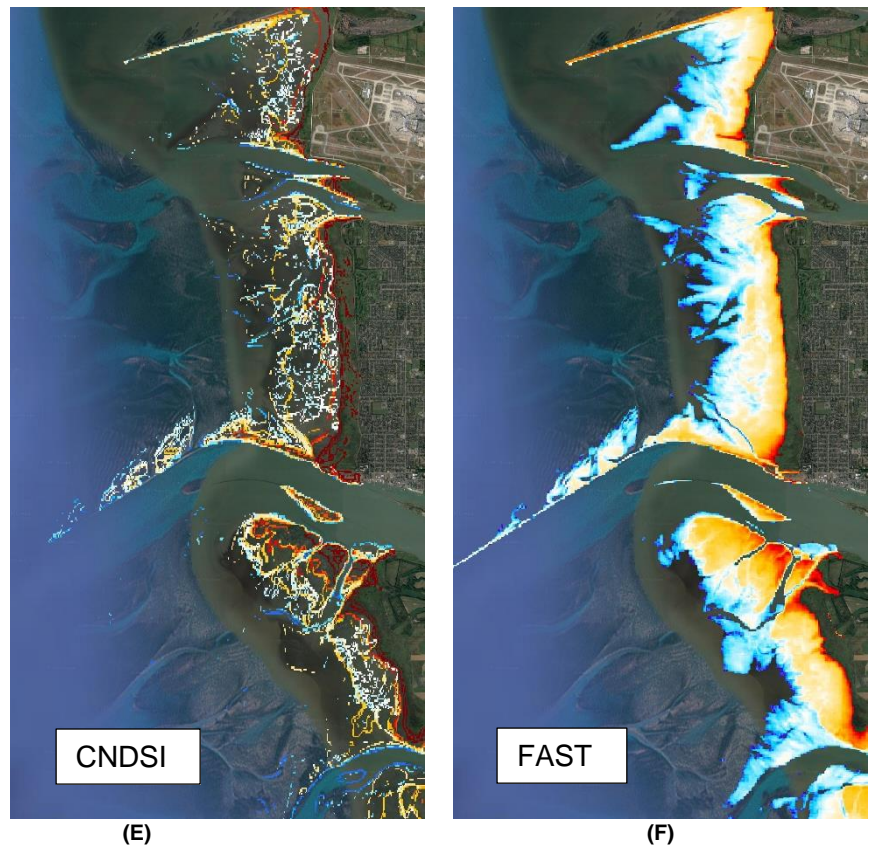


Figure 17 The selected FREMP transects for validating the results

3.1.2 Results

Elevations in the period 2008-2018





(E) (F)
Figure 18 The elevations from the LIDAR survey (A) and the elevations generated for the validation period 2008-2017 from satellite data. Maps B to E are generated by the water line method while F is generated by the FAST method

Random samples

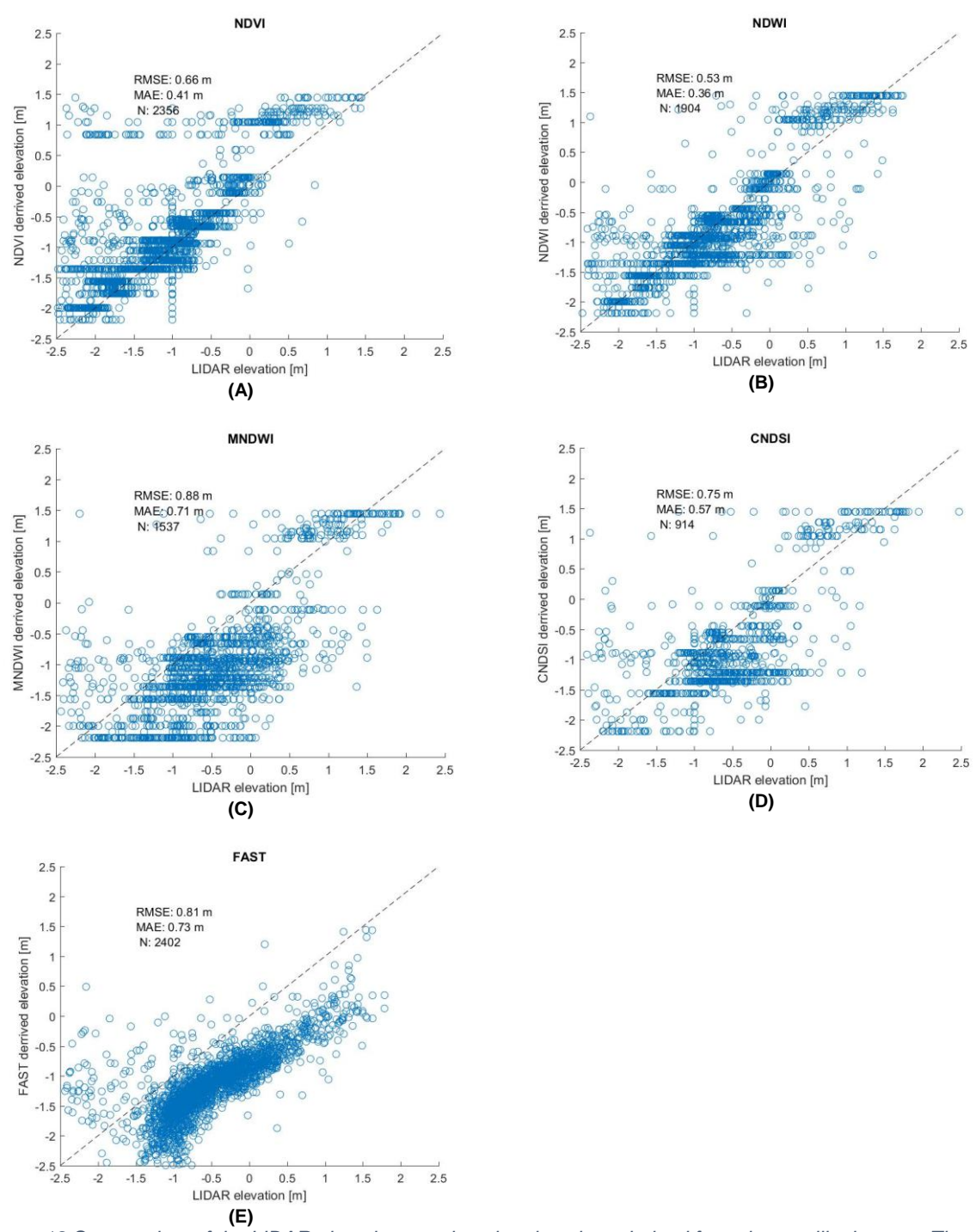


Figure 19 Scatter plots of the LIDAR elevations against the elevations derived from the satellite images. The water line method was carried out for the NDVI (A), NDWI (B), MNDWI (C), and CNDSI (D) indices. The FAST method (E) was carried out only once with the MNDWI.

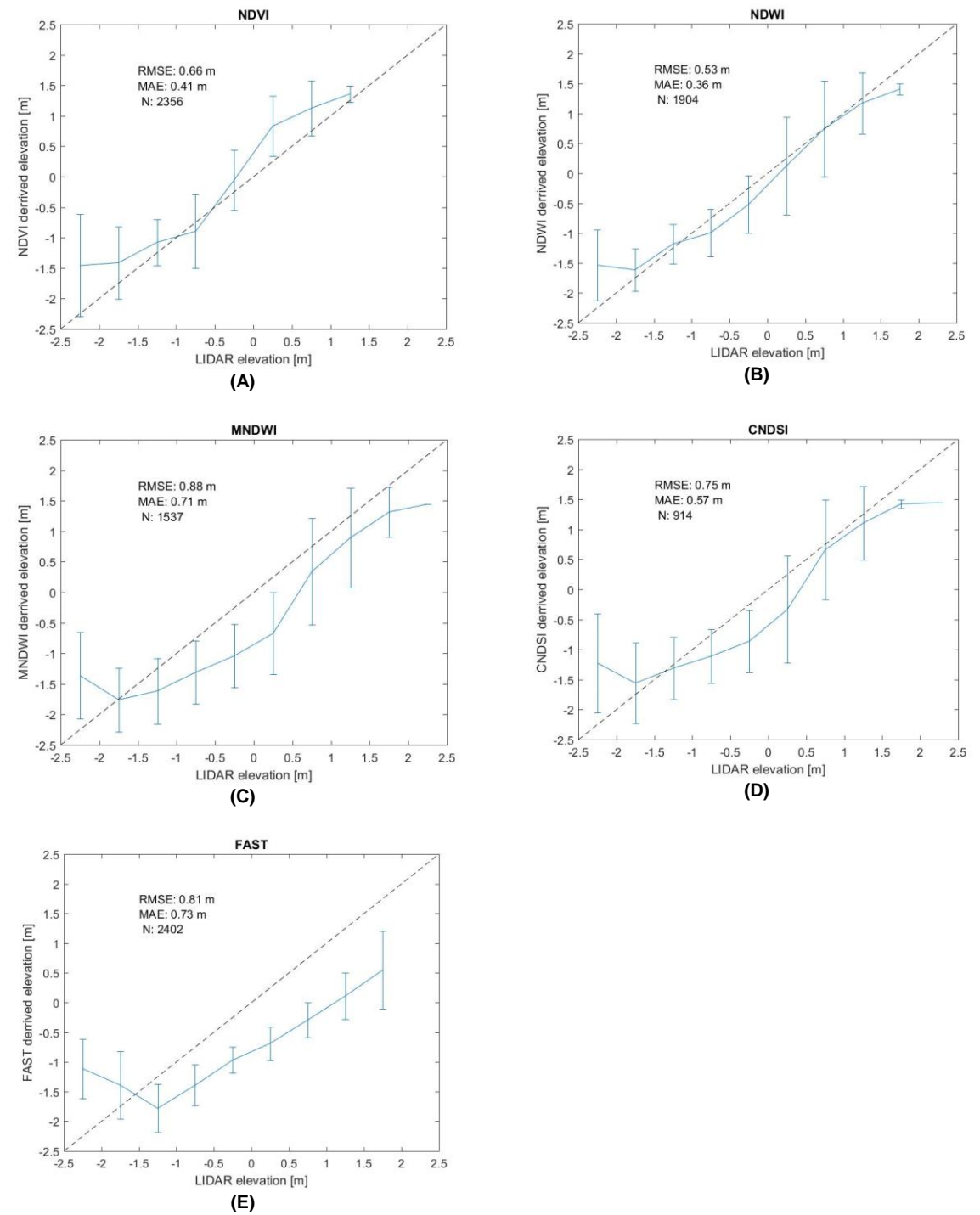


Figure 20 Graphs of the relation between the LIDAR elevations and the elevations derived from the satellite images. The line denotes the average satellite derived elevation for each LIDAR elevation while the error bar shows the standard deviation around the average. The water line method was carried out for the NDVI (A), NDWI (B), MNDWI (C), and CNDSI (D) indices. The FAST method (E) was carried out only once with the MNDWI.

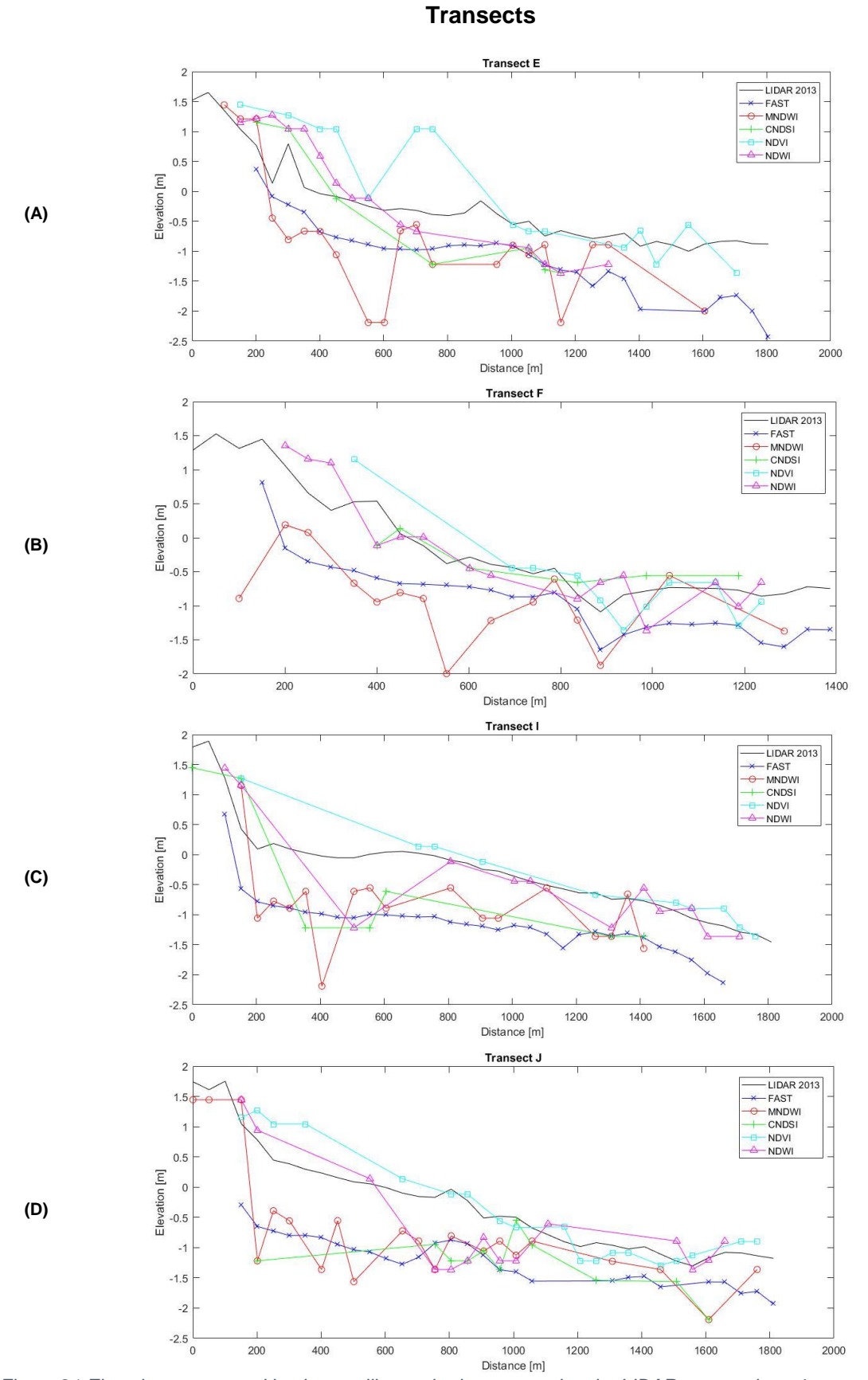


Figure 21 Elevations generated by the satellite methods compared to the LIDAR survey along 4 transects

Table 8 The root mean squared error and mean absolute error calculated for each method at each transect

		E		F		I		J
	RMSE	MAE	RMSE	MAE	RMSE	MAE	RMSE	MAE
FAST:	0.752	0.702	0.667	0.620	0.890	0.876	0.924	0.878
MNDWI:	0.925	0.727	1.017	0.859	0.887	0.764	0.892	0.738
CNDSI:	0.524	0.459	0.312	0.252	0.849	0.790	0.939	0.791
NDVI:	0.710	0.543	0.318	0.242	0.301	0.199	0.295	0.229
NDWI:	0.537	0.445	0.368	0.303	0.438	0.286	0.639	0.482

3.1.3 Discussion

All methods produce elevation maps that look similar to the LIDAR elevations (Figure 18). One advantage of the FAST method becomes immediately apparent which is the fact that it generates a full inter-tidal bathymetry, where the maps using the water line method leave gaps. It can also be observed that the NDVI method does contain noise as evidenced by the red specks seaward on figure 18B. The NDWI method shows noise as well in the Fraser River which, upon inspecting the original images, turns out to be the result of boats. This noise does not affect the elevations on the tidal flats for obvious reasons. The MNDWI and CNDSI are very similar in appearance. Both methods found more water lines shoreward compared to the other methods, but do not exhibit specks or stripes indicating noise. FAST produces on first sight a very detailed and credible elevations, but it can already be observed that elevations are structurally underestimated as compared to the LIDAR.

The figures 19 and 20 do show a clearer picture of the biases and errors of the methods. The methods all have a relatively high accuracy with the absolute errors ranging from 0.36 m to 0.73 m. The LIDAR itself can have an error in the order of up to 25 cm for this type of area (Hladik & Alber, 2012; Schmid, Hadley, & Wijekoon, 2011). The fact that these methods approach the accuracy with a much more limited resolution adds confidence to the viability of using satellite imagery for observing elevations.

As figure 19 shows, the scatter can be quite large. NDVI most notably shows large overestimations at low LIDAR elevations. This is most likely the result of the specks of noise that were visible in figure 18B. There is also another form of scatter at LIDAR elevations around and below -1 m across all methods. After inspecting the coordinates of the largest errors, it appears these originate from the channel in the south-eastern corner of Sturgeon Bank. The channel there is too thin to be detected by the resolution of the satellite and hence the much higher elevation surrounding it is detected. The large error is thus the result of the discrepancy in resolution. This discrepancy can also be responsible for rather large errors at the edges of other steep channel walls (e.g. at Swishwash island in between the airport and Sturgeon Bank), and to a lesser extent errors landward near the dike where the elevation gradient is steep compared to the flats.

Figures 18 and 19 further show a tendency of all methods to underestimate the elevations where the LIDAR elevation is above 1.5 m. The most likely reason is the presence of vegetation during winter and summer. The LIDAR survey was taken at the 23rd of July in summer and probably detected the top of the plants. The plants can grow upward of 1.2 m in the summer but die in autumn. If the elevation is estimated from a satellite image outside of the summer it can be expected that much lower elevations are found. Although this very likely the case, this problem warrants further verification in the field.

A final point of discussion is the structural underestimation of FAST. It should be noted that the MNDWI index used in FAST also does tend to underestimate elevations. Most likely the index is too sensitive to small puddles of water resulting in the underestimation. Either calibration or switching to a less biased index (e.g. NDWI) could have improved the method.

Further, the scaling of flooding probabilities linearly to elevations is not entirely accurate. As was shown in figure 7 of the tidal analysis, the relation between flooding and tidal elevation deviates far from a straight line which leads to underpredictions of the elevations up to 4 m+CD (or 1.8 m relative to mean sea level).

3.1.4 Best method

The best method should be the one that minimizes the error (i.e., low RMSE and MAE). In both figure 19 and figure 20 the best method should also be apparent as the method that is closest to a one-to-one relation with the LIDAR (dashed line), and does not have a large amount of scatter. Based on these criteria the water line method with the NDWI preformed the best with a RMSE of 0.53 m and MAE of 0.36 m. The scatter is low compared to the water line method with other indices and is well distributed around a one to one relation with the LIDAR.

Still the FAST method has advantages over the water line method. As figure 20 shows, the variation around the elevations is small. This becomes more apparent when looking at the transects that it produces (Figure 21) where the transects are much smoother. If the FAST method were recalibrated the transects would be superior to the transects produced by the other methods. It is expected that the bias remains constant throughout time and thus will not affect the elevation changes produced by the method. Because the ultimate objective of the study is to study elevation changes, rather than actual elevations, this method while uncalibrated will still be useable for that purpose.

The NDWI and FAST methods were both selected to analyse the full period of marsh recession. The NDWI water lines provide a better estimate of the elevations on the tidal flats, while FAST is used to study the elevation changes in greater detail.

3.2 Validation of the marsh extent



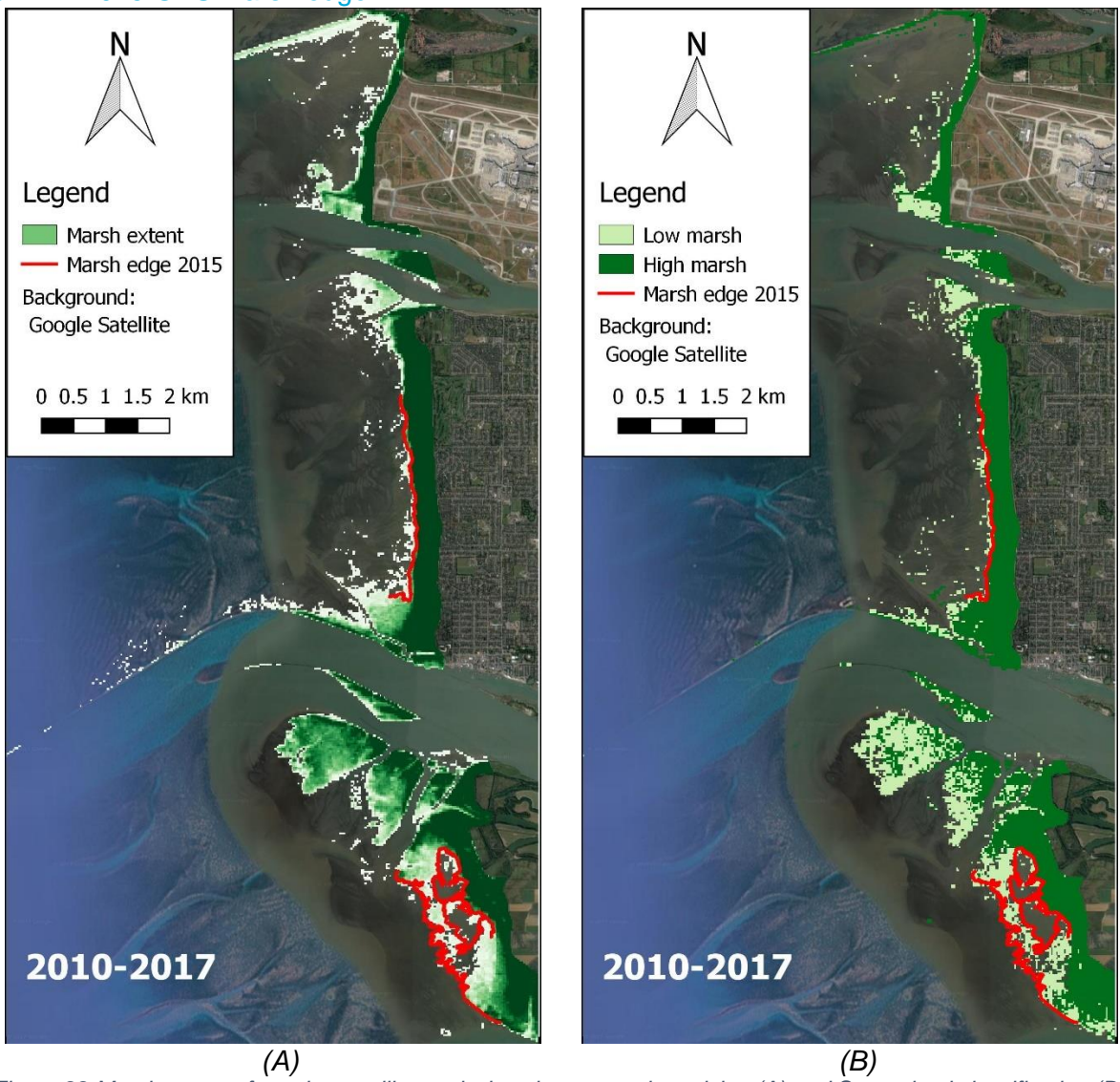


Figure 22 Marsh extents from the satellite analysis using spectral unmixing (A) and Supervised classification (B) compared to measured marsh extents by GPS by B. Mason (2016)

The marsh extends produced form the satellite imagery were verified against known marsh extents measured in the field in 2015-2016 by B. Mason (2016). The marsh leading edges had been measured during the summer of 2015 while the edge within the marsh was measured in 2016. The validation period was taken again as five years before and after the measurement. Because this study was carried out in 2017 the validation period was set to 2010-2017. All available images within this time were processed using the methodologies described in Chapter 2.6.

Both methods produce very similar marsh extents. The marsh edges match the observed marsh edges from 2015-2016 quite well. The edge on Sturgeon Bank is resembled more closely by the supervised classification where the biggest deviation from the edge was about 100 m (ignoring obvious noise), but most of the edge was followed within 1 pixel of variation (i.e., 30 m). Spectral unmixing preformed almost identical to the classification in the middle of Sturgeon Bank but misclassifies pixels about 300 m away from the edge in the southern end in a noisy pattern. It appears the cut-off for marsh in the spectral unmixing was set a little too loose as the slightly greener pixels delineate the marsh better.

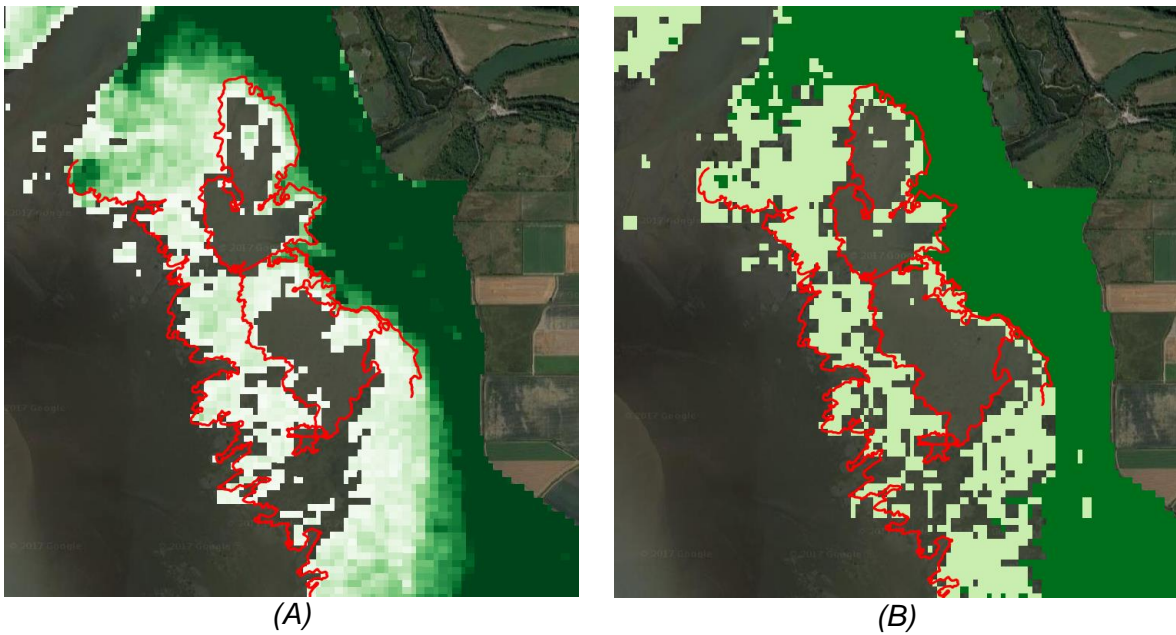


Figure 23 A close up of Westham island from figure 22 showing the marsh extents produced by spectral unmixing (A) and supervised classification (B) with the mars edge from 2015-2016 (red line) by B. Mason (2016).

On Westham Island there is bare flat within the marsh (nicknamed the "frog pond") that needs close verification. Both methods follow the outer edge of the marsh at the north end with great precession and one pixel of variation even picking up colonies of plants visible on the Google Earth background layer. At the southern outer edge however, a large area is identified as containing no or very little marsh by the unmixing method in particular. The spectral unmixing method also identifies a strip of marsh within the frog pond that the supervised classification correctly predicted as flat. Outside of these two areas however, spectral unmixing produced a more continuous marsh within the marsh edges while the supervised classification classified more individual pixels as bare flat.

3.2.2 1981 marsh survey

A large survey was conducted in 1981 looking at the composition and position of the marsh on Sturgeon Bank (W. S. Boyd, 1983). With this dataset the accuracy of the methods was tested on the marsh prior to the recession event. Satellite imagery was only available after 1980 from Landsat 5. To get enough images the validation period was chosen as 1980-1990. There is a risk that marsh recession started within this period, but differences are expected to be limited given the severe recession had been observed to have happened after 1989 (S. Boyd et al., *Unpublished*).

A simple check was performed for the validation: for each of the 124 sample points of the survey where a marsh species was documented, the satellite methods should indicate that point as marsh. The accuracy was calculated by counting the number of correctly identified sample points and dividing it by the total number of samples (Table 9).

Table 9 Accuracy of the marsh detection methods as calculated from the 1981 marsh survey samples from W. S. Boyd (1983)

N=124	Accuracy
Supervised classification	0.8629
Spectral unmixing	0.9032

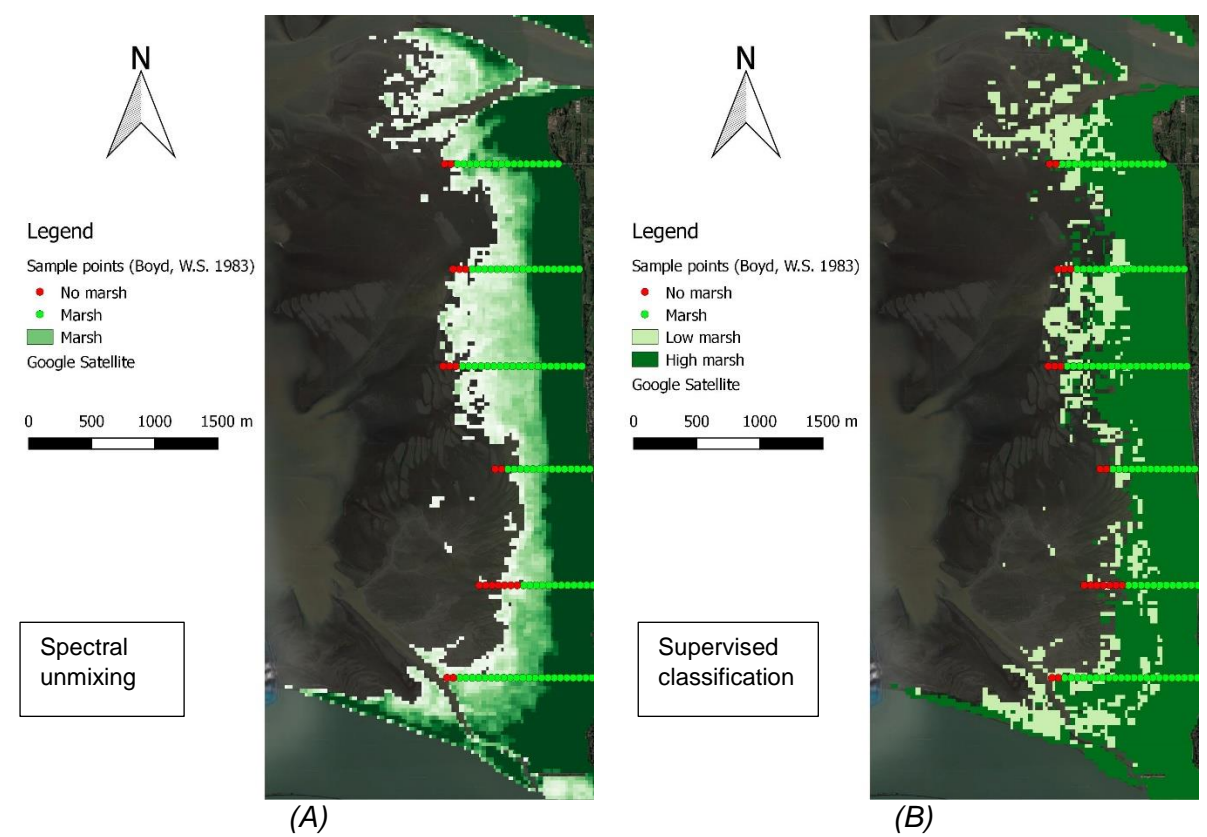


Figure 24 Comparison of the marsh survey in 1981 by W. S. Boyd (1983), compared to the results of the marsh detection for the period 1980-1990 by spectral unmixing (A) and supervised classification (B)

Both methods perform well with quite high accuracies of 86% for supervised classification and 90% for spectral unmixing. However with most of the sample points at the landward side of the marsh edge the performance is expected to be better as high marsh is more easily detected than the low marsh.

The low marsh is still quite accurately represented in both figure 24A and B. The transects in the north and middle are in almost perfect agreement with the survey. Most of the misclassifications occur in the two southernmost transects of Sturgeon Bank where more marsh is detected than was observed in the survey. Possibly this is due to the influence of the tidal channels in this area. As discussed in section 2.6, because (1) the algorithms learn to recognize the features from training areas and (2), the training areas for marsh tend to be higher in elevation and thus drier, the algorithms are implicitly trained to associate drier areas with marsh. The rapid dewatering through the tidal channels might thus incentive the algorithms to misclassify this area as marsh.

The spectral unmixing has calculated as having a 4% better accuracy than the supervised classification. Even though both methods perform similarly, the small gaps left within the marsh by the supervised classification where there should be marsh give the spectral unmixing a slight edge. Ignoring these, both methods are comparable in accuracy.

3.2.3 2017 field observation

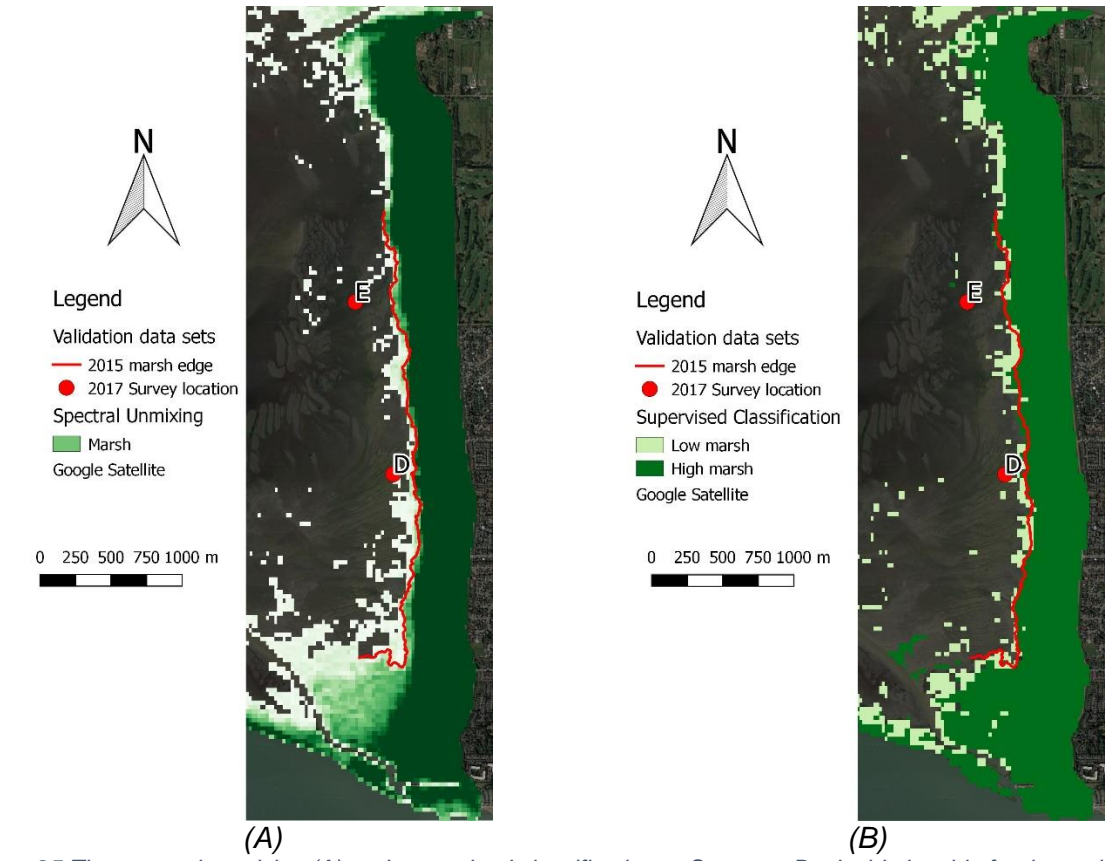


Figure 25 The spectral unmixing (A) and supervised classification at Sturgeon Bank side by side for the period 2010-2017 with the marsh edges by B. Mason (2016) and the location of the 2017 survey

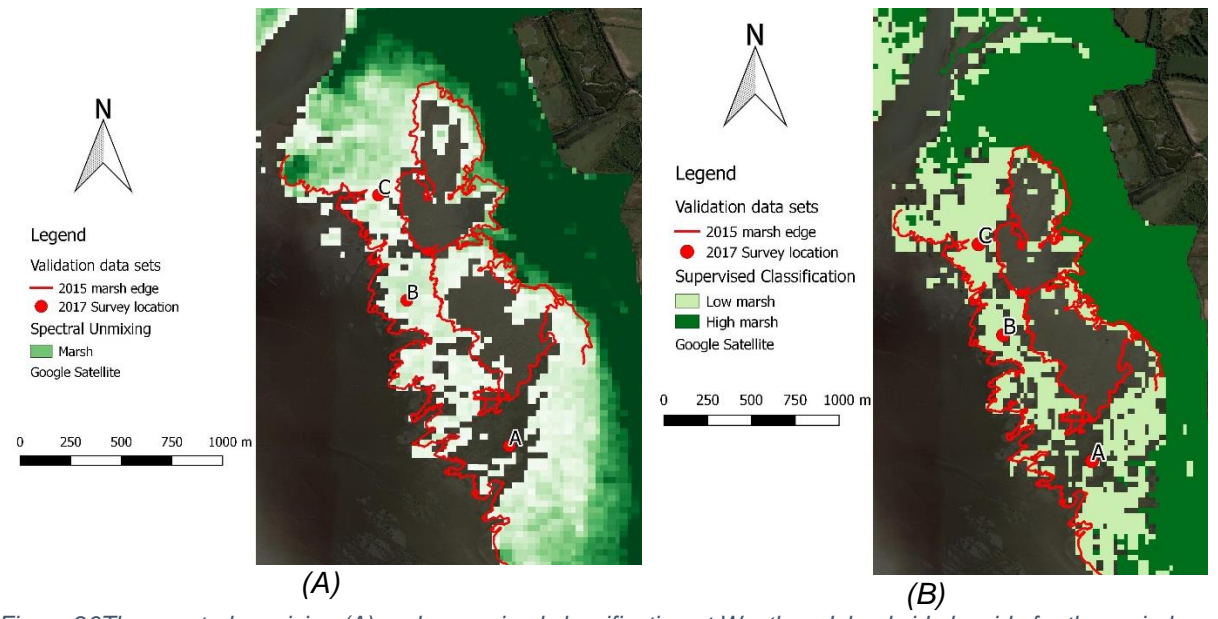


Figure 26The spectral unmixing (A) and supervised classification at Westham Island side by side for the period 2010-2017 with the marsh edges by B. Mason (2016) and the location of the 2017 survey

In the summer of 2017 Eric Balke surveyed 5 locations on Sturgeon Bank and Westham Island for this study to help interpret the results with *in situ* observations (see his field notes in Appendix: B). Five locations were selected where initial classification attempts showed conflicting results (see figure 25 and figure 26). At each location a 30 m x 30 m plot was made to mirror a 30 x 30m pixel from a satellite image. The area was photographed and the

type surface was recorded. In areas with marsh the fraction of area with vegetation within the plot was estimated.

The fractional cover of vegetation of the sample points was estimated as well from the results of the satellite images. By setting all marsh pixels to 1, and all detected bare flat pixels 0 within Google Earth Engine, the fraction of plant cover is estimated from the average value of all pixels in a 10-pixel radius around the sample point. For example, if in the area around the sample point half of the pixels is classified marsh and the other half is not, it can be assumed that within the pixel that is sampled half of the area is covered by plants. Although this is not necessarily true, it is a proxy to provide a first estimation of area plant cover. If a pixel is not classified as marsh while it should have, the cause might be that simply to little of the area was covered by too little vegetation to detect. Using the surveyed pixels from Eric Balke and the calculated plant cover proxies, this hypothesis is tested.

As table 10 shows, the plant cover proxies are similar to what was observed in the field. What becomes clear is that the areas on Westham Island where classification was difficult (A, B, C), the plant cover is estimated around the 50%. At location A the distribution of bulrush was observed to be very patchy. At location B almost the whole plot was covered by vegetation except for the large drainage channel running through it and the old grubbing holes from geese. Location C was observed to have a 4-cm deep pool in the middle of the plot. This sheds some light on the spatial difficulties of classification from low-resolution satellite images; it merges all the complex features within a 30x30m pixel into mixed signal. These pixels reveal that patchiness and the presence of water complicated a proper detection of the marsh.

On Sturgeon Bank the pixels of the survey would occasionally be misclassified as marsh. Although the proxy plant cover was low enough to not detect the pixel surveyed as marsh, there were still misclassified pixels around it. As noted by Eric, both locations D and E have non-native sea grass (*Zostera japonica*) and location E had 5% of its area covered by algae at the time of the survey. It is believed that algae deposition combined with the presence of sea grass can create a "green" enough spectral signature to lead to occasional false marsh classifications.

Table 10 Estimated plant cover from in-field observations, spectral unmixing and supervised classification

	In-field	Spectral unmixing		Supervised classification	
Point	Plant	Classified	Plant	Classified	Plant
	cover [%]	as marsh	cover [%]	as marsh	cover
					[%]
Α	50	No	34	No	37
В	85	Yes	62	Yes	56
С	60	Yes	71	Yes	70
D	1	No	30	No	21
Е	0	No	5	No	3

3.2.4 Discussion

The detection of marsh was performed well by both the spectral unmixing and the supervised classification. The predicted marsh extents are for most of the area in agreement with what was measured in 1981, 2015 and 2017 with a deviation of only 1 to 2 pixels.

The challenging areas proved to be the southern part of Sturgeon Bank and the marsh edge on Westham in front of the flat at the center of the marsh. At the very south of Sturgeon Bank the areas were misclassified as marsh but at Westham island marsh was misclassified as flat. The contrast between these two areas is the presence of water. While at Westham there was sparser marsh present with pooling water, the very south of Sturgeon Bank is drained quickly due to the larger system of tidal channels nearby. This drier flat is an exception as most of the flats are not drained as quickly. As discussed in section 2.6 the algorithms learn implicitly to see dryness as an attribute of the marsh since the marsh is generally higher in elevation and not inundated as much. Hence the difference between a dry flat and a marsh with ponds becomes more difficult to distinguish. The presence of plant matter is another attribute of marsh but when green algae and seagrasses are present the spectral signals of the two areas are even more similar.

It should be noted that these problems, while important, do not negate the high accuracy both methods demonstrated. Both methods were found to achieve comparable results with spectral unmxing having the slight advantage of showing a gradient in "marshness", rather than only a classification of high and low marsh.

4 Results and discussion

4.1 Tidal flat elevation

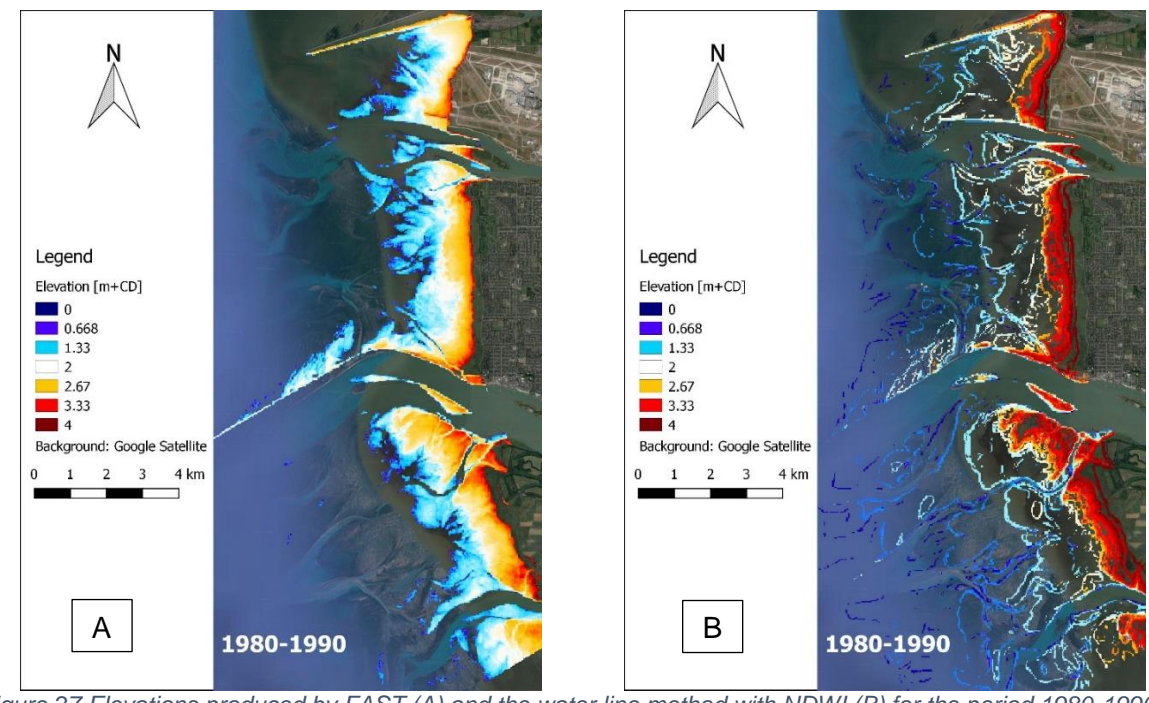


Figure 27 Elevations produced by FAST (A) and the water line method with NDWI (B) for the period 1980-1990

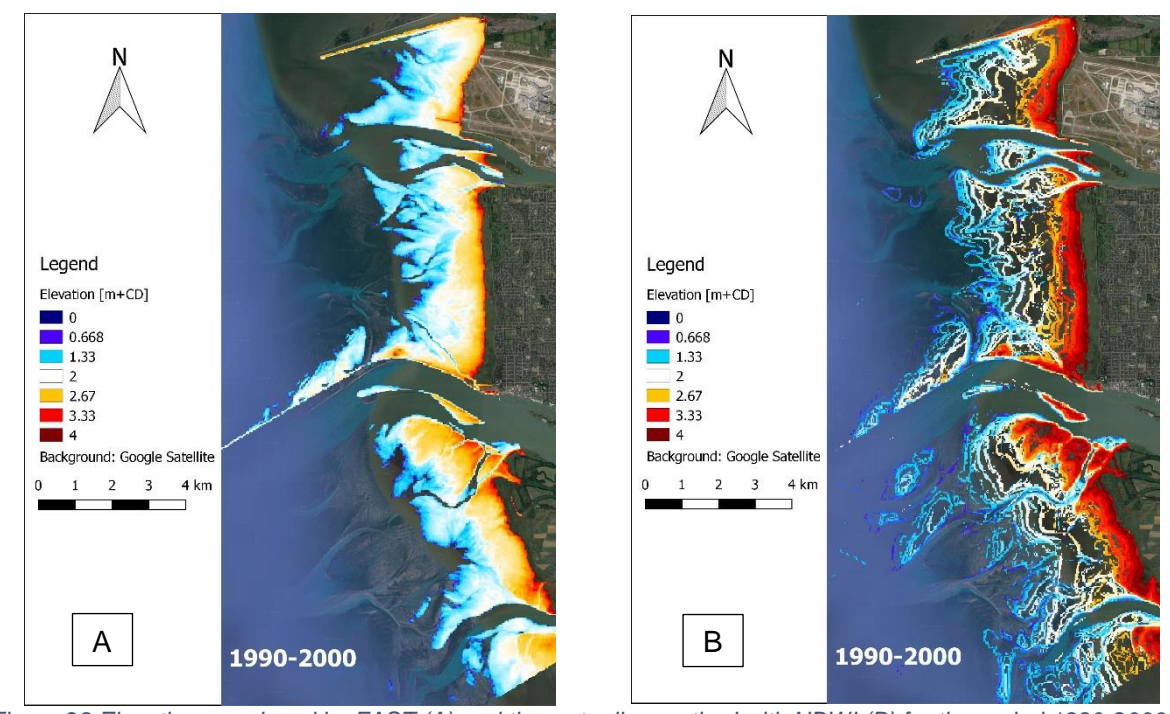


Figure 28 Elevations produced by FAST (A) and the water line method with NDWI (B) for the period 1990-2000

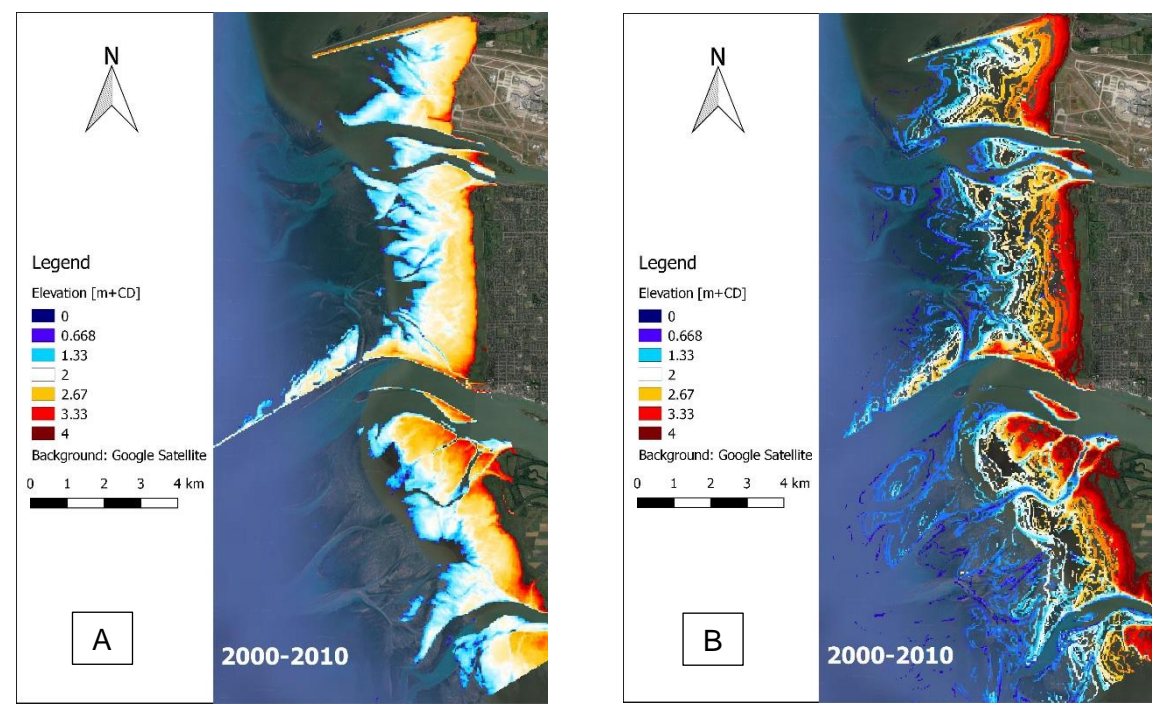


Figure 29 Elevations produced by FAST (A) and the water line method with NDWI (B) for the period 2000-2010

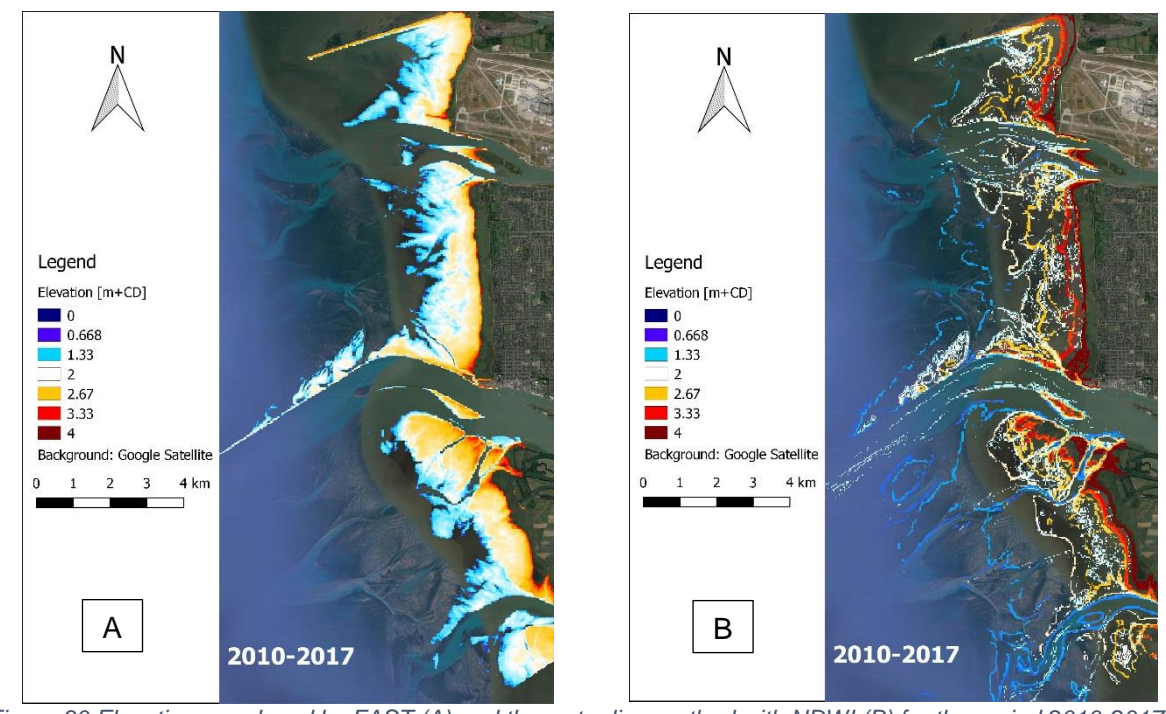


Figure 30 Elevations produced by FAST (A) and the water line method with NDWI (B) for the period 2010-2017

4.2 Marsh extent





Figure 31 Marsh extents produced by spectral unmixing (A) and supervised classfication (B) for the period 1980-1990





Figure 32 Marsh extents produced by spectral unmixing (A) and supervised classfication (B) for the period 1990-2000



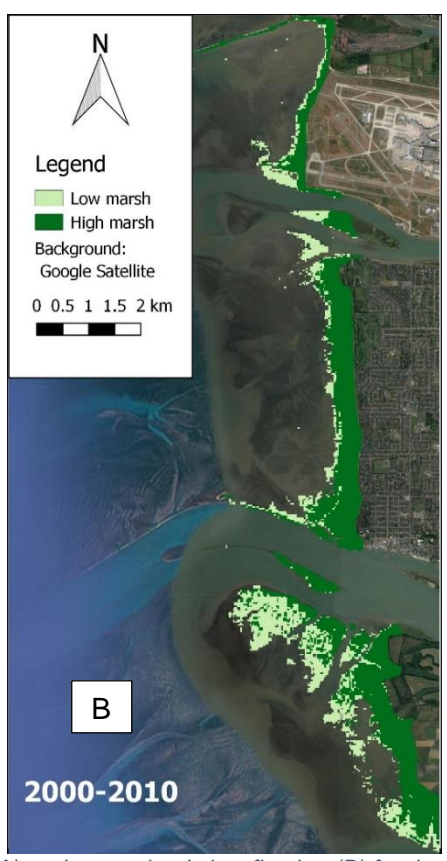


Figure 33 Marsh extents produced by spectral unmixing (A) and supervised classfication (B) for the period 1980-1990





Figure 34 Marsh extents produced by supervised spectral unmixing (A) and supervised classification (B) for the period 2010-2017

4.3 Marsh and elevation changes

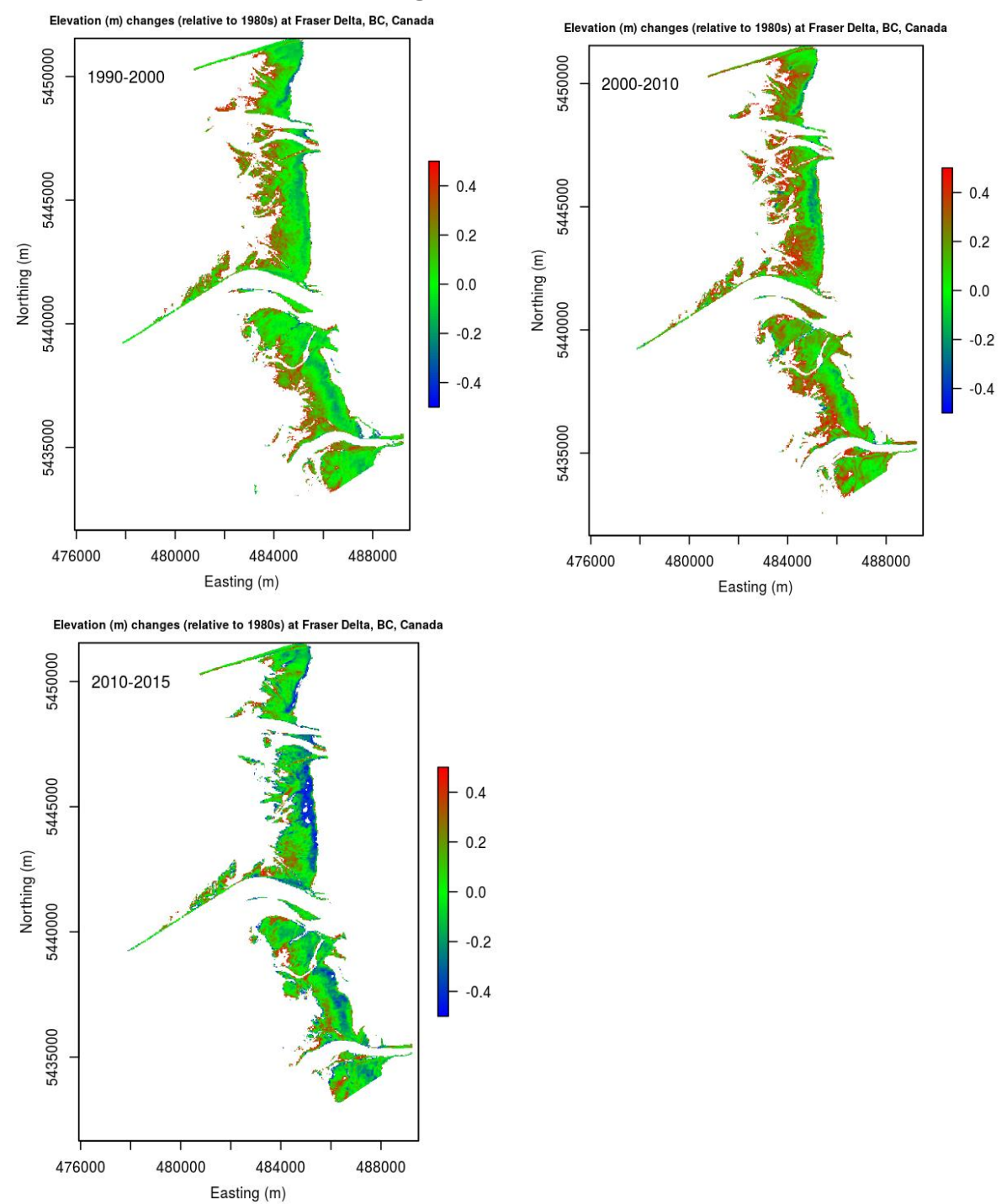


Figure 35 Elevation changes since 1980-1990 as calculated by FAST. Blue indicates a decrease in elevation, red an increase in elevation and green no change in elevation.

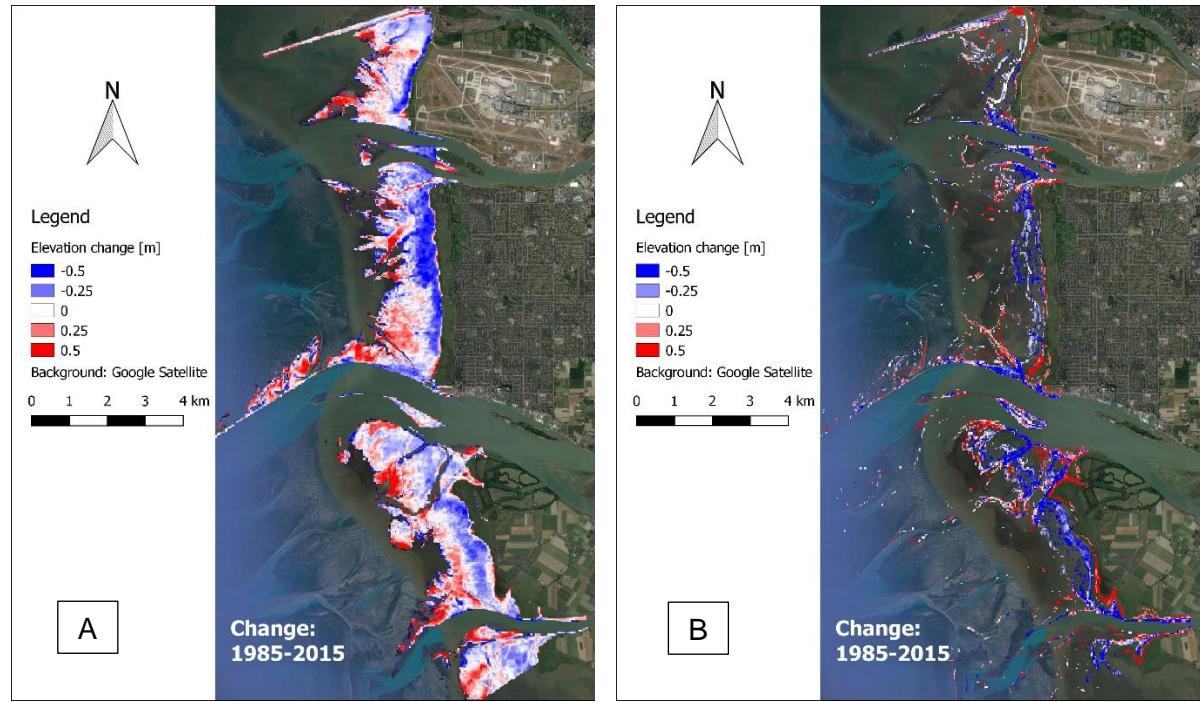


Figure 36 The elevation difference between the FAST elevation in 1980-1990 and 2010-2017 (A), and the elevation difference between the NDWI waterline elevation in 1980-1990 and 2010-2017 (B)

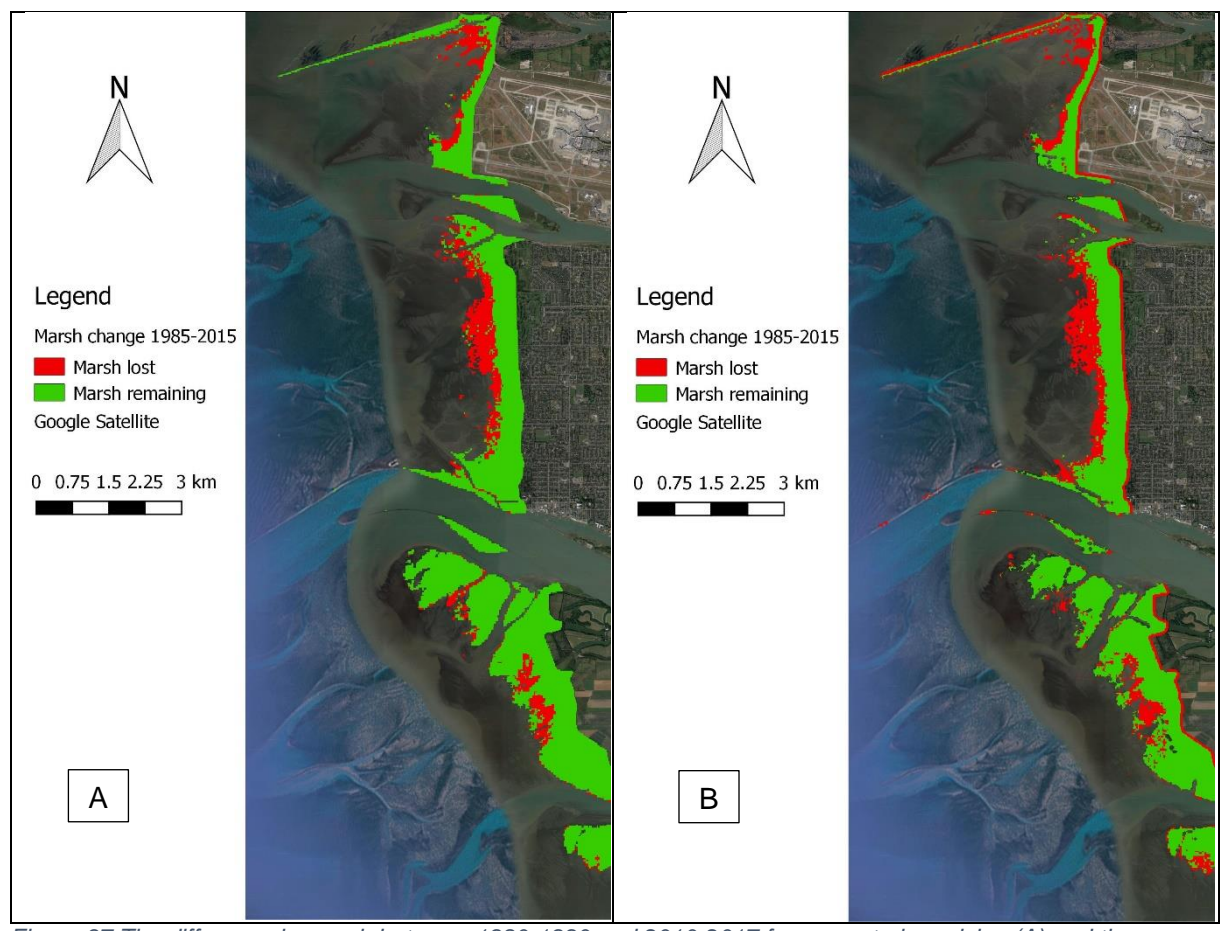


Figure 37 The difference in marsh between 1980-1990 and 2010-2017 from spectral unmixing (A) and the difference in marsh between 1980-1990 and 2010-2017 from supervised classification(B)

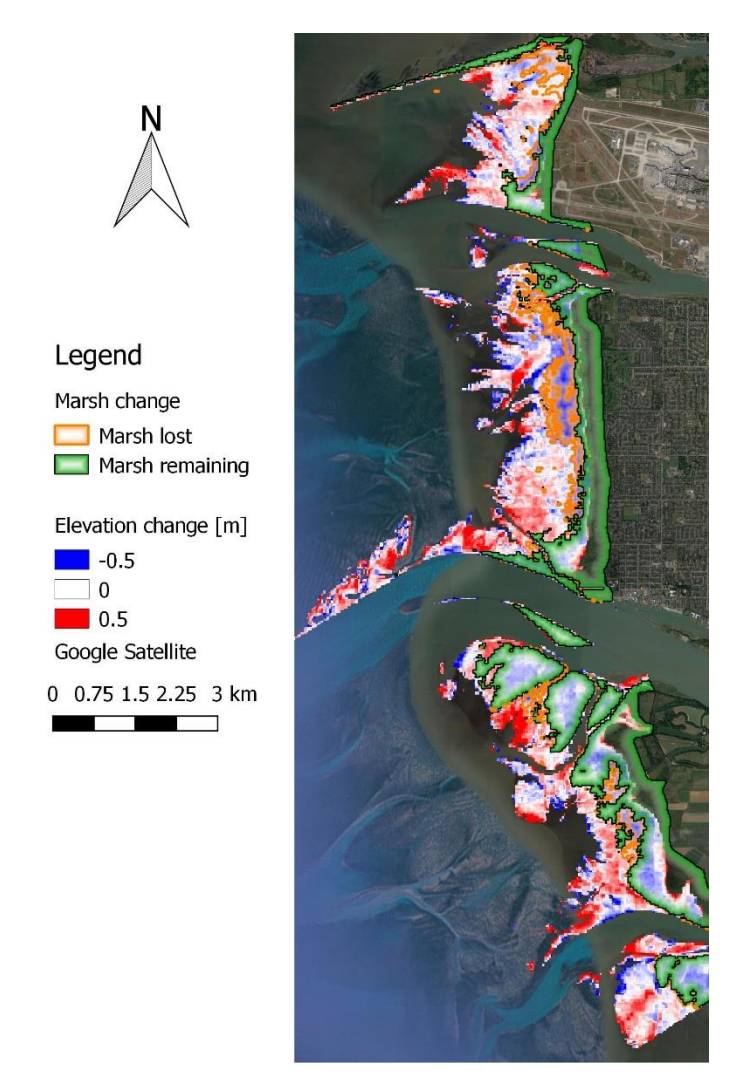


Figure 38 The marsh change from spectral unmixing from 1980-1990 to 200-2017 overlaid on top of the elevation change from FAST between 1980-1990 and 2010-2017

4.4 Discussion of the results

4.4.1 Tidal flat elevation

The tidal flat elevation did not change much for in the first years after 1980 to 2000, but the first signs of elevation loss start to become visible in the upper-part of the profile along the entire delta while an increase in elevation is detected seaward at the flats (Figure 27, Figure 28 and Figure 35). In the years after 2000 this trend continued (Figure 29 and Figure 35), though Sturgeon Bank is affected most. Further loss of elevation is detected in the years after 2010 (Figure 30 and Figure 35).

In figure 36 the total amount of elevation change is presented. It shows losses occurred along the upper-part of the profile roughly at the edge of the high marsh. On Sturgeon Bank this resulted in the loss of a slightly elevated plateau that existed in the 1980's while on Westham Island the loss occurred within the marsh itself. In fact, at the seaward leading edge on Westham no significant elevation changes were observed. At Sea island in front of YVR-airport loss of elevation is detected all the way to the dike.

The pattern of elevation loss along the upper-profile at each location suggests erosion could have occurred, caused by mechanisms affecting the entire Delta. These could be mechanisms like sea-level rise, storms, or any other process governing the coast on a regional scale. Research is needed to identify and quantify these mechanisms.

4.4.2 Marsh extent

In 1980-1990 the marsh at the center of Sturgeon Bank extended much further onto the flats than it does today (Figure 31). This had already been known from the comparing the leading edge survey in 2016 (B. Mason, 2016), to the 1981 marsh survey (W. S. Boyd, 1983) and the marsh survey by Hutchinson (1982) as well as the locations of corms found within the bare flat today (Balke, 2017). What had remained uncertain was when this marsh changed to its current state.

The results in figure 32 suggest this change started in the 1990's; a large portion of the marsh front receded on Sturgeon Bank and the marsh on Sea Island. On Westham Island the leading edge did not change significantly between 1980-1990 and 1990-2000, but within the marsh a bare flat started to form. In the period 2000-2010 these changes continue (Figure 33). The marsh on Stureon Bank receded until it was straignted, while on Westham Island the flat within the marsh expanded. After 2010 no more significant changes in marsh extent were observed (Figure 34).

The net change in marsh extent over the past 35 years is presented in figure 37. Most recession was observed on Sturgeon Bank, where the overall leading edge has receded by 200 m. At the center of Sturgeon Bank where the marsh was extending further outward 600 m of recession was observed to the point where the marsh no longer pretudes outward in this area. In total about 1.5 km² of marsh was lost on Sturgeon Bank. On Westham Island the leading edge has remained stable, but around 0.4 km² of marsh was converted to mud flat from the inside. These figures are close to estimations made by Balke (2017). Comparing leading edge and frog pond Trimble measurements by B. Mason (2016) to georeferenced air photos from 1979, Balke (2017) calculates that at least 1.6 km² of marsh has died off at Sturgeon Bank, and 0.55 km² low marsh died off and converted into mud flat from the inside sometime from 1989-2016.

4.4.3 Correlation between erosion and recession

One of the objectives of the study was to look for a correlation between the recession and the possible loss of sediment from the banks. If a sediment deficit is a contributing factor, indications should be found in the results.

The first period in which the marsh recession was observed was 1990-2000 and the recession appear to have stopped in by 2010-2017. No large elevation changes had been observed yet in 1990-2000. Most elevation changes were observed to have happened after 2000 up until the last period 2010-2017. The results indicate the elevation changes to be lagging behind the marsh changes and thus elevation changes are more likely to be caused by the loss of marsh rather than the other way around. As figure 38 shows, where marsh was lost on Sturgeon Bank the largest loss in elevation was detected. On Westham Island though, elevation loss was detected in both the lost marsh at the center, as well as within the remaining low marsh and no correlation was found.

As was discovered in the validation, the marsh has an influence on the predicted elevations from summer images by obscuring the water until it is high enough to be picked up through the stems. When marsh is lost, water is more easily detected, and the area would be identified as inundated earlier that if vegetation were present. As a result, some decrease in elevation at areas with marsh loss was expected. The validation could not quantify this effect. Erosion detected in these areas is likely a combination of this effect and actual erosion.

5 Summary and Conclusions

The use of satellite imagery to detect marsh and tidal changes proved an effective tool to shed new light on the marsh recession in the Fraser Delta. Two methods to calculate elevations from satellite imagery were employed and validated, the waterline method and a the method from the Foreshore Assessment using Space Technology-project (FAST) (FAST, 2017). All methods achieved higher than expected accuracies with mean absolute errors ranging from 0.36 m to 0.73 m. These accuracies are not far from the accuracy of the 2013 LIDAR survey provided by the Vancouver Fraser Port Authority used for validation, which is expected to be in the order of 20 cm in this environment (Hladik & Alber, 2012; Schmid et al., 2011). The largest errors were the result of the discrepancy in resolution between the LIDAR survey and the resolution of the satellite imagery which led to large elevations differences within channels that were to small to be detected by the satellite.

Erosion was detected by looking at the change in elevation from 1980 to 2017 at 10-year intervals. The elevations for each period were produced using the FAST method and the water line method. A limited amount of erosion was detected before 2000 but the largest amount of erosion was detected after 2000. It was concentrated at the upper-profile at 200 m from the dike on Sturgeon Bank and 600 m from the dike at Westham Island. Although elevation changes were in the order of -0.4 m, these are within the margin of error and no solid conclusions on the amount of erosion could be made. However, the consistent pattern of erosion across the entire delta front suggests erosion did take place and probably is the result of a process that affects the entire delta front.

The marsh was extracted from satellite imagery with the spectral unmixing technique and by using random forrest supervised classification. Both methods were validated against a 1981 marsh survey by W. S. Boyd (1983), the marsh edge as measured in the summers of 2015 and 2016 (B. Mason, 2016), and a field survey at five location in 2017 by Eric Balke. Both techniques performed similarly and achieved an accuracy within two satellite pixels (\pm 60m) for most of the area. Larger misclassifications were observed at the southern corner of Sturgeon Bank and the area in between the leading edge and inner mud flat on Westham Island. Factors leading to misclassifications were found to be: a small plant density, the pooling of water, the presence of sea-grass and algae.

The marsh extent for each 10-year period from 1980 to 2017 was produced by the supervised classification and spectral unmixing. The leading marsh edge on Sturgeon Bank receded rapidly between the periods 1980-1990 and 2000-2010, but showed no significant change after 2010. On Westham Island the outer leading edge remained stable, but marsh was being converted to mud flat in the same period as the marsh receded on Sturgeon Bank. Similarly, no large changes were detected on Westham after 2010. In total around 1.5 km² of marsh was lost along the leading of Sturgeon Bank and 0.4 km² of marsh was lost within the marsh on Westham Island.

The study did not find compelling evidence to support the hypothesis that erosion of sediments did lead to the loss of marsh along the Fraser Delta. Instead, the elevation changes appear to lag behind the loss marsh by one 10-year period. It is therefore more likely the marsh recession was a factor that lead to erosion, rather than the erosion leading to marsh recession.

6 References

- Atkins, R. J., Tidd, M., & Ruffo, G. (2016). Sturgeon Bank, Fraser River Delta, BC, Canada: 150 Years of Human Influences on Salt Marsh Sedimentation. *Journal of Coastal Research*, 75(sp1), 790-794. doi:10.2112/SI75-159.1
- Balke, E. (2017). Investigating the role of elevated salinity in the recession of a large brackish marsh in the Fraser River estuary. (Msc.), Simon Fraser University; British Columbia Institute of Technology
- Boyd, S., McKibbin, R., & Moore, K. (*Unpublished*). *The bulrush marshes of the Fraser River Delta have undergone significant changes between 1989 & 2011 (DRAFT)*.
- Boyd, W. S. (1983). Results of a 1981 Ecological Survey of the Lulu Island Foreshore Marshes.

 Unpublished. Canadian Wildlife Service, Pacific and Yukon Region, British Columbia. Delta,
 B.C.
- Breiman, L. (2001). Random Forests. *Machine Learning, 45*(1), 5-32. doi:10.1023/A:1010933404324 Chander, G., Markham, B. L., & Helder, D. L. (2009). Summary of current radiometric calibration coefficients for Landsat MSS, TM, ETM+, and EO-1 ALI sensors. *Remote Sensing of Environment, 113*(5), 893-903. doi:http://dx.doi.org/10.1016/j.rse.2009.01.007
- Church, M., & Hales, W. (2004). The Tidal Marshes of Fraser Delta: 75 years of Growth and Change. *Discovery*, *36*, 28-33.
- Donchyts, G., Baart, F., Winsemius, H., Gorelick, N., Kwadijk, J., & van de Giesen, N. (2016). Earth's surface water change over the past 30 years. *Nature Clim. Change, 6*(9), 810-813. doi:10.1038/nclimate3111
- FAST. (2017). The Science behind the MI-SAFE tool. Retrieved August 3 from https://publicwiki.deltares.nl/display/OET/The+Science+behind+the+MI-SAFE+tool
- Gorelick, N., Hancher, M., Dixon, M., Ilyushchenko, S., Thau, D., & Moore, R. (2017). Google Earth Engine: Planetary-scale geospatial analysis for everyone. *Remote Sensing of Environment*. doi:http://dx.doi.org/10.1016/j.rse.2017.06.031
- Hales, W. J. (2000). The Impact of Human Activity on Deltaic Sedimentation, Marshes of the Fraser River Delta, British Columbia. (Doctor of Philosophy), the university of British Columbia, Vancouver.
- Hardisky, M. A., Daiber, F. C., Roman, C. T., & Klemas, V. (1984). Remote sensing of biomass and annual net aerial primary productivity of a salt marsh. *Remote Sensing of Environment, 16*(2), 91-106. doi:http://dx.doi.org/10.1016/0034-4257(84)90055-5
- Herwig, C. (2016). Simple Cloud Score and Landsat 8. Retrieved from https://code.earthengine.google.com/3890321b866c5a24b7fde43256424885
- Hladik, C., & Alber, M. (2012). Accuracy assessment and correction of a LIDAR-derived salt marsh digital elevation model. *Remote Sensing of Environment, 121*, 224-235. doi:http://dx.doi.org/10.1016/j.rse.2012.01.018
- Housman, I. (2016). Simple cloud score and Landsat 8. https://groups.google.com/d/msg/google-earth-engine-developers/MCAO89Vj11Y/cOyOL3LBDAAJ
- Hutchinson, I. (1982). Vegetation—environment relations in a brackish marsh, Lulu Island, Richmond, B.C. *Canadian Journal of Botany*, *60*(4), 452-462. doi:10.1139/b82-061
- Irish, R. R. (1999, 2000). Landsat 7 automatic cloud cover assessment.
- Ma, L., Li, M., Ma, X., Cheng, L., Du, P., & Liu, Y. (2017). A review of supervised object-based land-cover image classification. *ISPRS Journal of Photogrammetry and Remote Sensing, 130*, 277-293. doi:http://dx.doi.org/10.1016/j.isprsjprs.2017.06.001
- Marijnissen, R. (2017). Potential mechanisms for the salt marsh recession on Sturgeon Bank. (Master of Science Master Thesis), TU Delft, Delft. Retrieved from http://repository.tudelft.nl/islandora/object/uuid:4fb116d6-39d4-46f9-ba4c-ac8f59e74549?collection=education

- Mason, B. (2016). GPS survey data of Sturgeon Bank and Westham Island marshes using Trimble Geo 7X handheld unit with Zephyr Model 2 Antenna. Unpublished data.
- Mason, D. C., Davenport, I. J., Robinson, G. J., Flather, R. A., & McCartney, B. S. (1995). Construction of an inter-tidal digital elevation model by the 'Water-Line' Method. *Geophysical Research Letters*, 22(23), 3187-3190. doi:10.1029/95GL03168
- McFeeters, S. K. (1996). The use of the Normalized Difference Water Index (NDWI) in the delineation of open water features. *International Journal of Remote Sensing*, *17*(7), 1425-1432. doi:10.1080/01431169608948714
- Medley, E., & Luternauer, J. L. (1976). *Use of aerial photographs to map sediment distribution and to identify historical changes on a tidal flat* Retrieved from http://edmedley.com/blog/wp-content/uploads/2008/06/medley-and-luternauer-1976.pdf
- Ministry of Forests, Lands and Natural Resource Operations. (2015). Sturgeon Bank Wildlife

 Management Area. Retrieved from http://www.env.gov.bc.ca/fw/habitat/conservation-lands/wma/sturgeon bank/
- Murray, N. J., Clemens, R. S., Phinn, S. R., Possingham, H. P., & Fuller, R. A. (2014). Tracking the rapid loss of tidal wetlands in the Yellow Sea. *Frontiers in Ecology and the Environment, 12*(5), 267-272. doi:10.1890/130260
- Richmond. (2005). *Heritage Inventory*. Retrieved from http://www.richmond.ca/plandev/planning2/heritage/HeritageInv/HeritageInventory.pdf
- Ryu, J.-H., Won, J.-S., & Min, K. D. (2002). Waterline extraction from Landsat TM data in a tidal flat. Remote Sensing of Environment, 83(3), 442-456. doi: http://dx.doi.org/10.1016/S0034-4257(02)00059-7
- Schmid, K. A., Hadley, B. C., & Wijekoon, N. (2011). Vertical Accuracy and Use of Topographic LIDAR Data in Coastal Marshes. *Journal of Coastal Research*, 116-132. doi:10.2112/JCOASTRES-D-10-00188.1
- Stephenson, A. G. (2016). Harmonic Analysis of Tides Using TideHarmonics. Retrieved from https://CRAN.R-project.org/package=TideHarmonics.
- Thomson, R. E. (1981). *Oceanography of the British Columbia Coast*. Ottowa: Department of Fisheries and Oceans.
- U.S. Geological Survey. (2015). Landsat—Earth observation satellites. Retrieved from www.usgs.com Van Der Meer, F. (1995). Spectral unmixing of Landsat Thematic Mapper data. International Journal of Remote Sensing, 16(16), 3189-3194. doi:10.1080/01431169508954622
- Williams, H. F. L., & Hamilton, T. S. (1995). Sedimentary Dynamics of an Eroding Tidal Marsh Derived from Stratigraphic Records of 137CS Fallout, Fraser Delta, British Columbia, Canada. *Journal of Coastal Research*, 11(4), 1145-1156.
- Xu, H. (2006). Modification of normalised difference water index (NDWI) to enhance open water features in remotely sensed imagery. *International Journal of Remote Sensing*, *27*(14), 3025-3033. doi:10.1080/01431160600589179
- Zhu, Z., Wang, S., & Woodcock, C. (2015). *Improvement and expansion of the Fmask algorithm: Cloud, cloud shadow, and snow detection for Landsats 4-7, 8, and Sentinel 2 images* (Vol. 159).

Appendix: A. Image dates and water levels

Image nr	Date [dd-MM-yyyy HH:mm]	Water level [m+CD]	Image nr	Date [dd-MM-yyyy HH:mm]	Water level [m+CD]
1	17-7-1984 18:36	2.61	79	15-10-1999 18:44	3.94
2	28-9-1984 18:31	3.66	80	13-2-2000 18:35	4.53
3	14-8-1985 18:31	0.96	81	17-4-2000 18:36	1.83
4	8-10-1985 18:36	3.25	82	28-6-2000 18:53	2.04
5	29-5-1986 18:25	3.17	83	30-7-2000 18:52	0.43
6	1-8-1986 18:23	1.65	84	22-8-2000 18:58	3.63
7	8-8-1986 18:29	2.22	85	23-8-2000 18:39	3.34
8	11-10-1986 18:27	3.5	86	23-9-2000 18:58	2.76
9	8-1-1987 18:20	4.26	87	24-9-2000 18:39	1.92
10	25-2-1987 18:22	3.5	88	10-11-2000 18:57	2.64
11	29-3-1987 18:23	1.94	89	22-1-2001 18:51	3.53
12	7-5-1987 18:31	2.97	90	4-4-2001 18:41	3
13	16-5-1987 18:25	1.88	91	20-4-2001 18:41	2.42
14	10-7-1987 18:32	0.33	92	21-5-2001 18:57	1.13
15	5-9-1987 18:28	1.04	93	22-5-2001 18:41	0.93
16	21-9-1987 18:28	1.63	94	9-7-2001 18:41	2.19
17	28-9-1987 18:34	4.04	95	25-7-2001 18:41	3.11
18	21-7-1988 18:32	3.18	96	10-8-2001 18:41	3.26
19	30-9-1988 18:38	4.2	97	26-8-2001 18:41	3.46
20	10-4-1989 18:36	2.69	98	4-10-2001 18:47	2.68
21	24-7-1989 18:28	3.45	99	12-7-2002 18:37	1.41
22	28-3-1990 18:27	1.83	100	13-8-2002 18:36	3.37
23	12-8-1990 18:21	3.76	101	5-9-2002 18:41	1.01
24	28-8-1990 18:21	3.41	102	21-9-2002 18:41	1.67
25	4-9-1990 18:27	1.34	103	22-9-2002 18:49	2.02
26	13-9-1990 18:21	2.92	104	16-10-2002 18:34	2.47
27	20-9-1990 18:27	2.61	105	1-11-2002 18:33	2.52
28	2-5-1991 18:29	2.14	106	12-2-2003 18:40	3.83
29	19-6-1991 18:30	3.2	107	1-9-2003 18:38	3.6
30	30-7-1991 18:24	2.62	108	4-11-2003 18:39	2.86
31	15-8-1991 18:24	3.83	109	11-3-2004 18:40	3.29
32	16-9-1991 18:25	3.44	110	28-4-2004 18:41	3.07
33	23-9-1991 18:31	1.92	111	17-7-2004 18:43	1.01
34	9-10-1991 18:31	3.09	112	24-7-2004 18:50	3.35
35	21-6-1992 18:30	2.98	113	2-8-2004 18:44	1.32
36	16-7-1992 18:24	1.77	114	9-8-2004 18:50	2.94
37	17-8-1992 18:23	3.08	115	18-8-2004 18:44	2.03
38	24-8-1992 18:30	1.9	116	17-2-2005 18:54	3.86
39	9-9-1992 18:29	1.61	117	22-4-2005 18:54	1.83
40	16-2-1993 18:29	3.61	118	20-7-2005 18:49	0.46

41	25-2-1993 18:23	3.33	119	27-7-2005 18:55	3.51
42	23-5-1993 18:30	1.66	120	5-8-2005 18:49	1.15
43	4-8-1993 18:23	2.16	121	21-8-2005 18:49	1.57
44	12-9-1993 18:29	2.17	122	6-9-2005 18:49	2.55
45	24-11-1993 18:23	3.29	123	4-5-2006 18:53	3.02
46	3-5-1994 18:21	3.16	124	28-6-2006 19:00	1.58
47	20-6-1994 18:20	1.34	125	23-7-2006 18:54	0.91
48	22-7-1994 18:19	0.91	126	31-8-2006 19:01	3.67
49	30-8-1994 18:24	3.08	127	25-9-2006 18:55	3.13
50	24-9-1994 18:17	3.85	128	2-10-2006 19:01	3.19
51	1-10-1994 18:23	2.53	129	11-10-2006 18:55	4.33
52	3-3-1995 18:12	3.14	130	14-5-2007 19:02	1.53
53	26-3-1995 18:17	3.03	131	30-5-2007 19:01	1.09
54	13-5-1995 18:15	1.1	132	10-7-2007 18:55	2.12
55	30-6-1995 18:13	2.16	133	26-7-2007 18:55	1.77
56	16-7-1995 18:12	2.94	134	19-9-2007 19:00	3.79
57	29-10-1995 18:00	4.51	135	5-10-2007 19:00	3.3
58	2-2-1996 18:06	3.26	136	12-7-2008 18:48	2.52
59	11-7-1996 18:15	1.57	137	4-8-2008 18:53	2.29
60	27-7-1996 18:16	1.42	138	14-9-2008 18:46	1.47
61	12-8-1996 18:17	1.29	139	28-5-2009 18:49	2.27
62	18-12-1996 18:23	4.31	140	4-6-2009 18:55	1.62
63	4-2-1997 18:26	3.67	141	13-6-2009 18:49	2.77
64	11-5-1997 18:29	2.78	142	16-8-2009 18:50	2.27
65	18-5-1997 18:36	2.11	143	24-9-2009 18:57	4.15
66	7-9-1997 18:39	1.59	144	9-7-2010 18:58	1.25
67	23-9-1997 18:40	1.48	145	25-7-2010 18:58	0.93
68	18-3-1998 18:44	3.28	146	6-10-2010 18:51	2.03
69	2-8-1998 18:39	2.72	147	13-10-2010 18:57	4.45
70	3-9-1998 18:40	1.78	148	23-4-2011 18:57	3.02
71	26-9-1998 18:46	3.81	149	5-7-2011 18:50	2.56
72	21-10-1998 18:40	2.83	150	7-9-2011 18:50	2.55
73	15-4-1999 18:40	1.45	151	16-10-2011 18:55	3.89
74	22-4-1999 18:46	3.41	152	4-10-2015 19:20	4.38
75	12-7-1999 18:54	0.43	153	11-9-2016 19:23	3.21
76	28-7-1999 18:54	1.13	154	7-12-2016 19:18	4.44
77	13-9-1999 18:44	3.08	155	30-3-2017 19:20	2.07
78	22-9-1999 18:37	1.82	156	29-5-2017 19:27	1.84

Appendix: B. Pixel survey June, July 2017

Below are the field notes and pictures from Eric Balke of his survey in the summer of 2017.

Plot A

- <u>location</u>: 10 U, 0486251 E, 5436710 N

- survey date: 06 July 2017

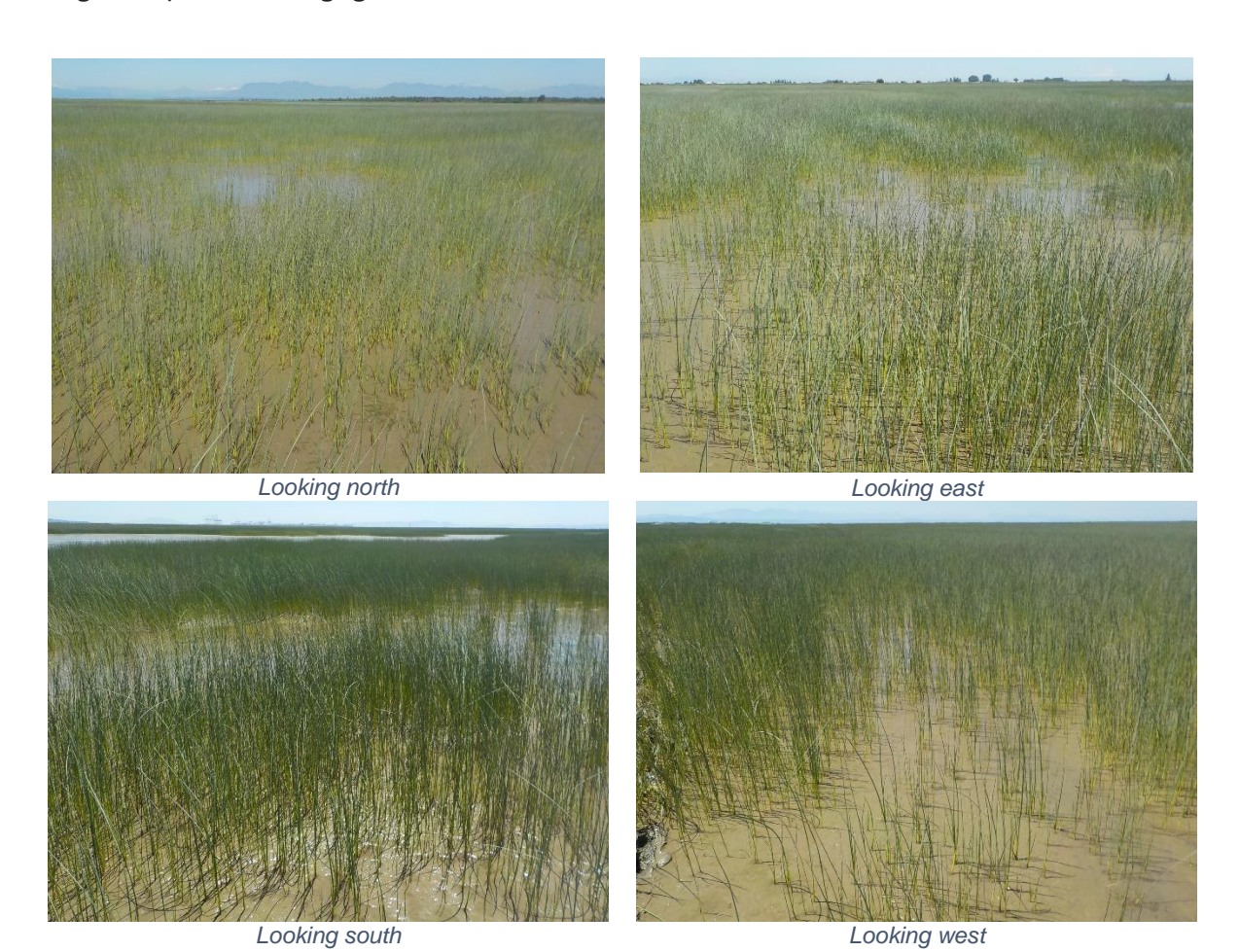
- weather: sunny

- substrate: slightly muddy

- water: some pooling in depressions

- <u>vegetation cover</u>: ~50% *Schoenoplectus pungens* in a highly variable, patchy distribution; located just north of a large area of mud flat (i.e., denuded marsh)

- <u>algae deposition</u>: negligible





In the middle looking west

Plot B

- <u>location</u>: 10 U, 0485749 E, 5437423 N

- survey date: 06 July 2017

- weather: sunny

- substrate: slightly muddy

- water: some pooling in depressions

- <u>vegetation cover</u>: ~80-90% *S. pungens*; old goose grubbing holes and large drainage channel constitute unvegetated proportion

- algae deposition: negligible







Looking east





Looking south

Looking west



In the middle looking west

Plot C

- <u>location</u>: 10 U, 0485605 E, 5437946 N

- survey date: 06 July 2017

- weather: sunny

- substrate: slightly muddy

- water: up to 4 cm pooling in large denuded pool in middle of plot

- <u>vegetation cover</u>: ~60% *S. pungens*; large denuded pool with *Ruppia maritima* (widgeon grass) in the middle of the plot; large mudflat immediately south of plot.

- algae deposition: negligible



In the middle looking west

Plot D

- location: 10 U, 0485270 E, 5443727 N

- survey date: 28 June 2017

- weather: sunny

- substrate: mud flat with recent deposition of mud over lots of plot

- water: approximately 0-1 cm pooling water throughout plot

- <u>vegetation cover</u>: <5% *Zostera japonica* (likely greater, but much of area has recent deposition of mud), ~10 shoots of *S. pungens*

- <u>algae deposition</u>: negligible



Plot E

- location: 10 U, 0485003 E, 5444940 N

- survey date: 28 June 2017

<u>weather</u>: sunny<u>substrate</u>: mud flat

- water: approximately 1 cm pooling water throughout plot

vegetation cover: 10% Z. japonicaalgae deposition: <5% Ulva lactuca

